Examensarbete

Simulation of Heat Transfer on a Gas Sensor Component

Rebecka Domeij Bäckryd

LITH - MAT - EX - - 05/10 - - SE

Simulation of Heat Transfer on a Gas Sensor Component

Department of Mathematics, Linköpings Universitet

Rebecka Domeij Bäckryd

LITH - MAT - EX - - 05/10 - - SE

Examensarbete: **20 p**

Level: **D**

Supervisors: **Mikael Löfdahl**,
AppliedSensor
Dan Loyd,
Applied Thermodynamics and Fluid Mechanics,
Department of Mechanical Engineering,
Linköpings Universitet

Examiner: **Lars Eldén**,
Numerical Analysis,
Department of Mathematics,
Linköpings Universitet

Linköping: **May 2005**

LINKÖPINGS UNIVERSITET

Avdelning, Institution
Division, Department

Matematiska Institutionen
581 83 LINKÖPING
SWEDEN

Datum
Date

May 2005

Språk
Language

☐ Svenska/Swedish
☒ Engelska/English
☐ _____

Rapporttyp
Report category

☐ Licentiatavhandling
☒ Examensarbete
☐ C-uppsats
☐ D-uppsats
☐ Övrig rapport
☐ _____

ISBN

ISRN
LITH - MAT - EX - - 05/10 - - SE

Serietitel och serienummer **ISSN**
Title of series, numbering

URL för elektronisk version
http://www.ep.liu.se/exjobb/mai/2005/na/010/

Titel
Title

Simulation of Heat Transfer on a Gas Sensor Component

Författare
Author

Rebecka Domeij Bäckryd

Sammanfattning
Abstract

Gas sensors are today used in many different application areas, and one growing future market is battery operated sensors. As many gas sensor components are heated, one major limit of the operation time is caused by the power dissipated as heat. AppliedSensor is a company that develops and produces gas sensor components, modules and solutions, among which battery operated gas sensors are one targeted market.

The aim of the diploma work has been to simulate the heat transfer on a hydrogen gas sensor component and its closest surroundings consisting of a carrier mounted on a printed circuit board. The component is heated in order to improve the performance of the gas sensing element.

Power dissipation occurs by all three modes of heat transfer; conduction from the component through bond wires and carrier to the printed circuit board as well as convection and radiation from all the surfaces. It is of interest to AppliedSensor to understand which factors influence the heat transfer. This knowledge will be used to improve different aspects of the gas sensor, such as the power consumption.

Modeling and simulation have been performed in FEMLAB, a tool for solving partial differential equations by the finite element method. The sensor system has been defined by the geometry and the material properties of the objects. The system of partial differential equations, consisting of the heat equation describing conduction and boundary conditions specifying convection and radiation, was solved and the solution was validated against experimental data.

The convection increases with the increase of hydrogen concentration. A great effort was made to finding a model for the convection. Two different approaches were taken, the first based on known theory from the area and the second on experimental data. When the first method was compared to experiments, it turned out that the theory was insufficient to describe this small system involving hydrogen, which was an unexpected but interesting result. The second method matched the experiments well. For the continuation of the project at the company, a better model of the convection would be a great improvement.

Nyckelord
Keyword

Gas Sensor, Heat Transfer, Conduction, Convection, Convection Coefficient, Partial Differential Equation, Finite Element Method and FEMLAB.

Abstract

Gas sensors are today used in many different application areas, and one growing future market is battery operated sensors. As many gas sensor components are heated, one major limit of the operation time is caused by the power dissipated as heat. AppliedSensor is a company that develops and produces gas sensor components, modules and solutions, among which battery operated gas sensors are one targeted market.

The aim of the diploma work has been to simulate the heat transfer on a hydrogen gas sensor component and its closest surroundings consisting of a carrier mounted on a printed circuit board. The component is heated in order to improve the performance of the gas sensing element.

Power dissipation occurs by all three modes of heat transfer; conduction from the component through bond wires and carrier to the printed circuit board as well as convection and radiation from all the surfaces. It is of interest to AppliedSensor to understand which factors influence the heat transfer. This knowledge will be used to improve different aspects of the gas sensor, such as the power consumption.

Modeling and simulation have been performed in FEMLAB, a tool for solving partial differential equations by the finite element method. The sensor system has been defined by the geometry and the material properties of the objects. The system of partial differential equations, consisting of the heat equation describing conduction and boundary conditions specifying convection and radiation, was solved and the solution was validated against experimental data.

The convection increases with the increase of hydrogen concentration. A great effort was made to finding a model for the convection. Two different approaches were taken, the first based on known theory from the area and the second on experimental data. When the first method was compared to experiments, it turned out that the theory was insufficient to describe this small system involving hydrogen, which was an unexpected but interesting result. The second method matched the experiments well. For the continuation of the project at the company, a better model of the convection would be a great improvement.

Keywords: Gas Sensor, Heat Transfer, Conduction, Convection, Convection Coefficient, Partial Differential Equation, Finite Element Method and FEMLAB.

Acknowledgements

My examiner, Lars Eldén, has been an important support throughout this project. Dan Loyd became my supervisor at the university, and his knowledge in the area of heat transfer and willingness to help, have been very valuable to me. I would like to thank both of you for being engaged in all my questions.

Mikael Löfdahl, my supervisor at AppliedSensor, made this diploma work possible. Daniel Tenselius and Jonas Widén deserve my thanks for helping me performing the experiments. There are many other people at the company who have shown an interest in my work, and I especially want to mention Tom Artursson and Gunnar Karlström.

Linus Andersson and Peter Georen at FEMLAB Support have patiently answered my questions on how to use FEMLAB as a tool for solving heat transfer problems in general and my problem in particular.

I would also like to give my gratitude to David Lawrence for helping me computing gas properties for mixtures and giving input on how to calculate the convection coefficient.

Vedran Bandalo, thanks for being my opponent, for reading and questioning my work.

Last of all, I would like to thank Emmanuel. Thank you for being my support in life.

Nomenclature

Symbols and abbreviations are described here. SI units are used throughout the report, except for temperature that is given in degrees Celsius when convenient.

Symbols

T	temperature [K]
t	time [s]
x	x-axis in cartesian coordinate system
y	y-axis in cartesian coordinate system
z	z-axis in cartesian coordinate system
$\boldsymbol{n}$	normal vector
N_2	concentration of nitrogen gas in volume fraction [%]
O_2	concentration of oxygen gas in volume fraction [%]
H_2	concentration of hydrogen gas in volume fraction [%]
P	power [W]
$\dot{Q}$	rate of heat flow [W]
$\dot{q}$	rate of heat flow per unit of area (scalar) [W/m^2]
$\dot{\boldsymbol{q}}$	rate of heat flow per unit of area (vector) [W/m^2]
$\dot{g}$	rate of heat generation per unit of volume [W/m^3]
h	convection coefficient [W/m^{2}K]
ρ	density [kg/m^3]
c_p	specific heat capacity at constant pressure [J/kgK]
k	thermal conductivity (scalar) [W/mK]
$\boldsymbol{k}$	thermal conductivity (matrix) [W/mK]
σ	Stefan-Boltzmann constant [W/m^{2}K^4]
ϵ	emissivity
μ	viscosity [kg/ms]
x^v	volume fraction
x^n	mole fraction
x^m	mass fraction
M	molar mass [kg/mole]
T_{bi}	normal boiling point [K]
A	area [m^2]
v	test function
N_i	basis function
$\boldsymbol{K}$	stiffness matrix
$\boldsymbol{f}$	force vector

g	gravitational acceleration [m/s^2]
X	characteristic length [m]
β	coefficient of volumetric thermal expansion [1/K]
Gr	Grashof number
Pr	Prandtl number
Nu	Nusselt number

Abbreviations

PDE	Partial Differential Equation
FEM	Finite Element Method
PCB	Printed Circuit Board

Contents

Chapter 1

Introduction

In this diploma work, simulation of heat transfer on a gas sensor component will be performed. The introduction covers a presentation of the problem, the background, basic concepts of heat transfer, the method used to solve the problem and an outline of the report.

1.1 Presentation of the Problem

The aim of the diploma work is to provide an understanding of the heat transfer on a hydrogen gas sensor component and its closest surroundings for steady-state conditions. This knowledge will be used to improve some aspects of a hydrogen gas sensor, developed at the company AppliedSensor.

The gas sensor component consists of a silicon chip. There are several elements on the chip; heaters, a temperature sensor and a gas sensor element. The chip is heated in order to improve the features of the gas sensor element on the chip. The temperature sensor is used to keep the temperature stable by feed-back coupling to the heaters. The chip is placed on a glass carrier that is placed on a PCB. The glass carrier provides thermal insulation between the chip and the PCB, which is important in order to minimize the power dissipation of the sensor component. The chip is connected to the PCB through bond wires. In figure 1.1, the chip, the glass carrier and the bond wires are shown.

Heat transfer occurs by conduction from the chip, through the glass carrier and the bond wires, to the PCB, as well as convection and radiation from all the surfaces to the surrounding gas. The amount of heat transfer by convection increases with the hydrogen concentration, implying an increased power consumption to maintain a constant chip temperature.

Theories from the areas of heat transfer, physics, numerical analysis and mathematics are used throughout the diploma work. Some assumptions and simplifications are made in order to solve a complex, realistic problem.

The diploma work is part of a larger project in which a fundamental understanding of the heat transfer on the gas sensor component and its surroundings is searched for. It includes heat transfer for steady-state conditions as well as

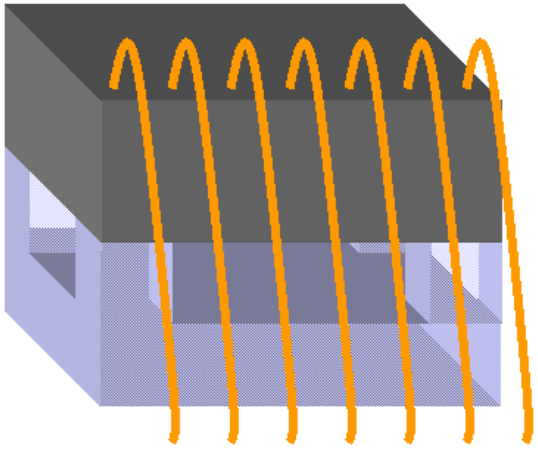

Figure 1.1: The chip placed on the glass carrier and the bond wires connecting the chip to the PCB.

for time-dependent conditions. It is important to understand which factors influence the power dissipation of the sensor component in order to minimize the power consumption. The geometry of the chip, the glass carrier and the bond wires, the orientation of the sensor module, the material properties, water vapor and the presence of other gases are factors that need to be examined.

1.2 Background

The diploma work has been performed at AppliedSensor, a company that was established in the year 2000 through the fusion of the two companies Nordic Sensor Technologies in Sweden and MoTech in Germany. Nordic Sensor Technologies was formed as a spin-off from the university in Linköping, and there is still a close connection between the company and research carried out in the gas sensor area at the university.

Since 2001, AppliedSensor focuses on development and production of gas sensor components, modules and solutions based on three main principles; metal oxide semiconductor sensors, field effect sensors and quartz microbalance sensors [2]. The company provides unique gas sensor solutions in the areas of air quality, control and safety for major OEMs[1]. One growing future market is battery operated sensors. As many gas sensor components are heated, one major limit of the operation time is caused by the power dissipated as heat, which is why heat transfer is interesting to study.

The gas sensor examined in this project is a hydrogen gas sensor. Experiments have been performed before the start of the diploma work, in order to obtain an understanding of the distribution of heat transfer between conduction through

[1] OEM stands for Original Equipment Manufacturer.

the glass carrier, conduction through the bond wires as well as convection and radiation from the surfaces of the chip to the surrounding gas.

In the experiments, the chip temperature was kept constant at 140°C and the module was surrounded by air in room temperature (approximately 20°C). It is important to note however, that these experiments were performed on an older version of the gas sensor module than the version studied here, and that the bond wires and glass carrier were attached to a gold header instead of a PCB. The obtained figures are therefore not completely reliable for the module and set-up studied in this diploma work, but gives an idea of the distribution.

The power input to the heaters was measured for a chip placed on the glass carrier and a chip suspended by the bond wires and hence hanging freely in the air, see figures 1.2 and 1.3. The experiment was performed for steady-state conditions, and therefore the total power input to the heaters was equal the sum of conduction, convection and radiation from the chip.

The power input for the suspended chip and the chip on the glass carrier was measured. The power increase from the suspended to the non suspended chip was due to conduction through the glass carrier. The number of bond wires was then reduced from seven to five, and the heat transfer by conduction through the bond wires could be calculated. The part of the power input that was not lost by conduction, was lost by convection and radiation to the air. The result is presented in figures 1.2 and 1.3. The fraction of heat flow by conduction through the glass carrier was 46% and through the bond wires 22%. Further, the fraction of heat flow by convection and radiation to the air was 32%.

1.3 Heat Transfer

A general definition of heat transfer is the following: "Heat transfer [...] is thermal energy in transit due to a temperature difference" [12, p.2]. There are three different modes of heat transfer: conduction, convection and radiation.

1.3.1 Conduction

Heat transfer through solids and stationary fluids due to a temperature difference is called conduction [12]. Energy is transferred from a region of higher temperature to a region of lower temperature. The heat flow from the sensor chip through the glass carrier and the bond wires to the PCB is caused by conduction.

The physical mechanism of conduction is due to the energy exchange between molecules and/or atoms in a solid or stationary fluid (gas or liquid). In a gas for example, the particles in a region of higher temperature transfer energy to particles in a region of lower temperature through a process of random motion [12].

The expressions for the rate of heat flow per unit of area for each mode of heat transfer are called rate equations [12]. The rate equation for conduction is the so called Fourier's law [14]:

$$\dot{\boldsymbol{q}}_{conduction} = -\boldsymbol{k}\nabla T \ , \tag{1.1}$$

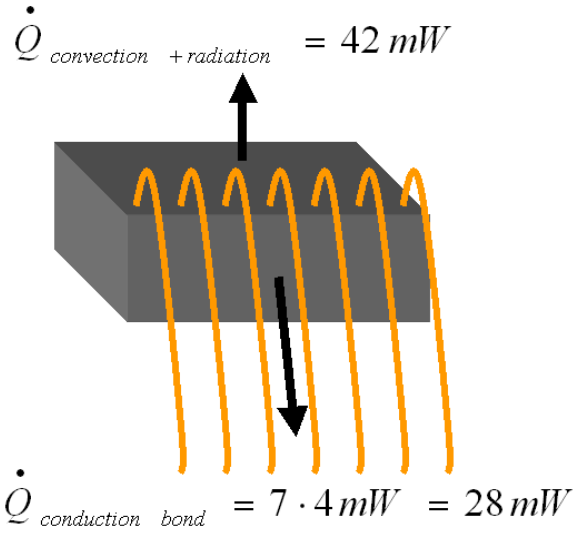

Figure 1.2: Heat flow from the chip suspended by the bond wires.

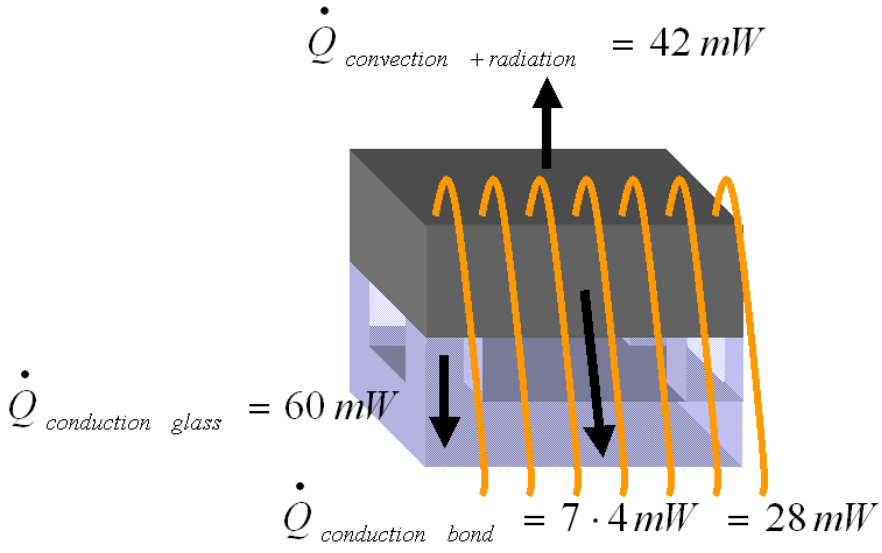

Figure 1.3: Heat flow from the chip on the glass carrier.

where $\dot{\boldsymbol{q}}_{conduction}$ is a vector representing the heat flow per unit of area, $\boldsymbol{k}$ is the thermal conductivity, T is the temperature and ∇T is the gradient of the temperature. In three dimensions, the equation can be written as [14]:

$$\dot{\boldsymbol{q}}_{conduction} = - \begin{pmatrix} k_{xx} & k_{xy} & k_{xz} \\ k_{yx} & k_{yy} & k_{yz} \\ k_{zx} & k_{zy} & k_{zz} \end{pmatrix} \begin{pmatrix} \frac{\partial T}{\partial x} \\ \frac{\partial T}{\partial y} \\ \frac{\partial T}{\partial z} \end{pmatrix} . \tag{1.2}$$

1.3.2 Convection

Convection describes heat that is transferred between a solid surface and the surrounding fluid. Heat flows from the surface of the sensor chip, the glass carrier and the PCB to the surrounding gas through convection.

Convection is partly a mechanism of conduction and partly a mechanism of fluid motion. In other words, apart from the random motion of particles in conduction described in section 1.3.1, "energy is also transferred by the bulk, or macroscopic, motion of the fluid" [12, p.6].

There are two different types of convection; forced convection and natural (or free) convection. In forced convection, the bulk motion of the fluid is caused by some external means, such as a fan or the wind. In natural convection on the other hand, the motion of the fluid is caused by the gravitational force. There is a density gradient in a fluid with a temperature gradient. The gravitational force makes the denser part fall and the less dense part rise. This is what happens on a horizontal, hot surface exposed to a cold fluid; the fluid close to the surface is heated by the surface, becomes less dense and rises at the same time as the colder fluid falls and takes its place [6].

Newton's law of cooling is the rate equation for convection [12]:

$$\dot{q}_{convection} = h(T_{surface} - T_{fluid}) , \tag{1.3}$$

where $\dot{q}$ is the heat flow from the surface in the direction normal to the surface, h is the convection coefficient, $T_{surface}$ is the temperature of the surface and T_{fluid} is the temperature of the fluid.

1.3.3 Radiation

Radiation is the third mode of heat transfer in which energy is transferred by electromagnetic waves. It is the only mode that does not need an intervening medium. When studying radiation as a heat transfer mode, we are interested in thermal radiation, which is radiation emitted by matter with temperatures above zero Kelvin [6]. Heat flow through radiation occurs together with convection from the surfaces of the chip, the glass carriers and the PCB to the surrounding gas.

"Radiation is a *volumetric phenomenon*, and all solids, liquids, and gases emit, absorb, or transmit radiation to varying degrees. However, radiation is usually considered to be a *surface phenomenon* for solids that are opaque to thermal radiation such as metals [...] since the radiation emitted by the interior regions

of such material can never reach the surface, and the radiation incident on such bodies is usually absorbed within a few microns from the surface" [6, p.613].

The radiation emitted from a surface is based on the Stefan-Boltzmann law and is given by [6]:

$$\dot{q}_{radiation} = \epsilon\sigma T^4_{surface} \ , \tag{1.4}$$

where $\dot{q}$ is the heat flow from the surface in the direction normal to the surface, ϵ is the emissivity of the surface, σ is the Stefan-Boltzmann constant and $T_{surface}$ is the temperature of the surface.

To obtain the rate equation for radiation, we assume that the surface is surrounded by a much larger surface with temperature $T_{ambient}$ and that the gas between the two surfaces does not intervene with radiation. The net radiation from the smaller surface is then the radiation emitted minus the radiation absorbed due to the emission from the larger surface. The rate equation can then be expressed as [12]:

$$\dot{q}_{radiation} = \epsilon\sigma(T^4_{surface} - T^4_{ambient}) \ . \tag{1.5}$$

1.3.4 Heat Transfer by Conduction, Convection and Radiation

The three different modes of heat transfer often occur simultaneously. In figure 1.4, a simple system shows the three mechanisms. An oblong solid body with temperature T_2 is attached to a large solid body with temperature T_1. T_1 is higher than T_2, causing a heat flow by conduction from the large solid to the oblong solid. Both solids are surrounded by air with the temperature T_3. T_3 is lower than T_2 and T_1. Heat is transferred from the surfaces of the solids to the surrounding air by convection and radiation.

1.4 Method

The system that is to be modeled consists of the chip, the glass carrier, the bond wires, the PCB and the surrounding gas. Certain assumptions and simplifications are made. The most important simplification is to restrict the sensor model to the chip, the glass carrier, the bond wires and a part of the PCB. The surrounding gas is modeled as a boundary to the system, which implies that the dynamics of the gas is not considered. The first main step is to describe the system, including the geometry, the material properties and the properties of the surrounding gas.

All three modes of heat transfer occur in the sensor system or at its boundaries. There is conduction within the solid domains, which can be described by the so called heat equation in each domain. This results in a set of PDEs. At all surfaces of the system, heat transfer occurs through convection and radiation, which is described by boundary conditions to the PDEs.

To find an appropriate convection coefficient is usually a difficult task that will be approached in two different ways; a semi-empirical and an empirical method. In the semi-empirical approach, formulas for the convection coefficient found in

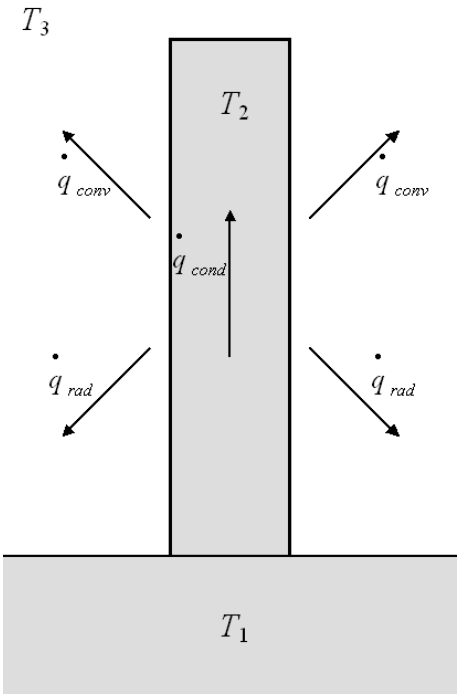

Figure 1.4: The three different modes of heat transfer occurring simultaneously, $T_1 > T_2 > T_3$.

the literature are used. These are not based only on fundamental principles, but obtained from systematic studies of the behaviour of convection on different surfaces. As the formulas are not purely empirical, but developed with a theoretic understanding of convection, the method is called semi-empirical in this report. The empirical approach does not take into account the theories developed for the convection coefficient. Instead, it takes experimental data from the sensor component as the starting point for finding the convection coefficient, which gives a model that is valid only for the experimental conditions.

The PDEs with the corresponding boundary conditions will be solved using the software FEMLAB 3.1 for the semi-empirical and the empirical model. FEMLAB is a tool for modeling and solving problems described by PDEs using the finite element method. The solutions will be compared with experimental data and the validity of the models will be discussed.

1.5 Outline of the Report

The main topics dealt with are presented in the chapters below.

Chapter 2: The sensor system is described.

Chapter 3: The heat equation and the boundary conditions are defined.

Chapter 4: The basics of the finite element method are presented.

Chapter 5: The experimental setup, plan and data, needed to validate the models, are accounted for.

Chapter 6: A semi-empirical model of the convection coefficient is defined. After the model has been implemented and the equations have been solved in FEMLAB with MATLAB, described in chapter 9, the result is compared to experimental data.

Chapter 7: An empirical model of the convection coefficient is defined. The result is compared to experimental data.

Chapter 8: The implementation of the models in FEMLAB with MATLAB is accounted for.

Chapter 9: Conclusion of the diploma work and an overview of future work are presented.

Chapter 2

Sensor System

In this chapter, the geometry and the material properties of the sensor system, as well as the properties of the possible gas compositions in the vicinity of the sensor are described. Furthermore, a parameter range definition, assumptions and simplifications and a model of the sensor system are accounted for.

2.1 Geometry

The gas sensor component consists of a silicon chip on which the following elements are placed:

- Heaters
- Temperature sensor
- Gas sensor element

The heaters are made of five transistors. The power input to the heaters is regulated by external electronics on the PCB so that the temperature measured by the temperature sensor is kept constant. The gas sensor element measures the hydrogen concentration in the vicinity. In figure 2.1, the dimensions of the chip and the positions of the elements mentioned in the list above are specified.

The chip is placed on a glass carrier that provides thermal insulation between the chip and the PCB. The dimensions of the glass carrier are specified in figure 2.2.

A three dimensional picture of the chip, the glass carrier and the bond wires is given in figure 2.3. A coordinate system is specified to simplify the presentation. The origin is placed in the lower left corner of the glass carrier.

There are seven bond wires connecting the chip to the PCB. The bond wires are formed as cylinders. They have radius 12.5 μm, approximate length 1.5 mm and are attached to pads drawn as squares at the lower end of the chip in figure 2.1. The length of the bond wires is difficult to measure, which creates

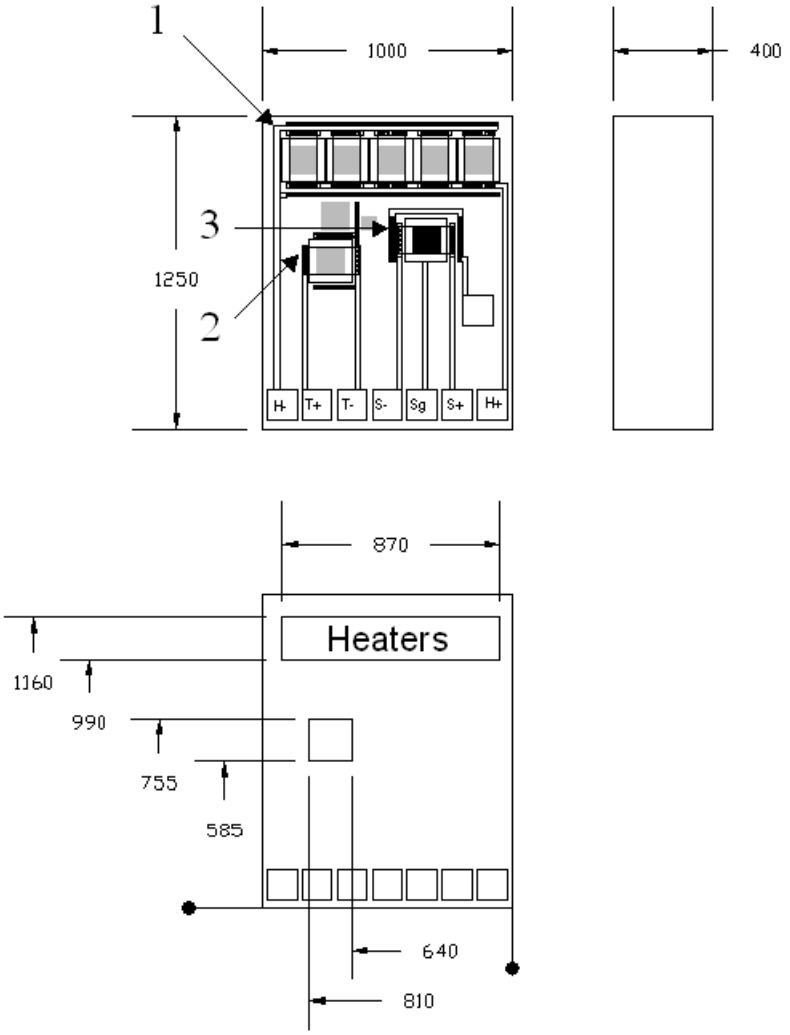

Figure 2.1: The dimensions of the chip (μm). 1=heaters, 2=temperature sensor and 3=gas sensor element.

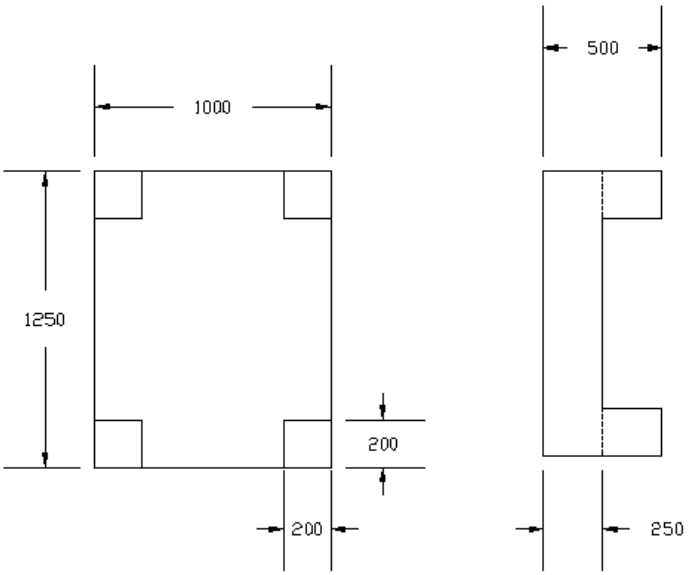

Figure 2.2: The dimensions of the glass carrier (μm).

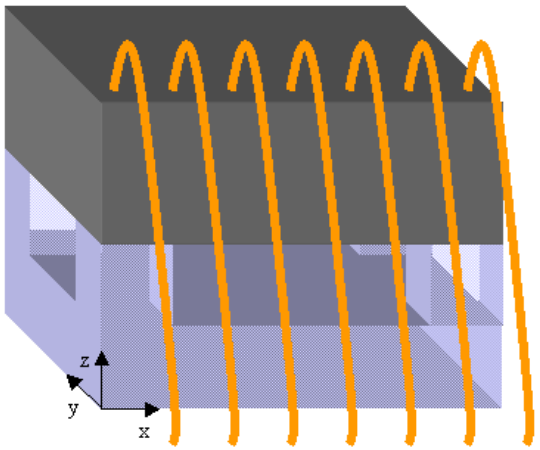

Figure 2.3: The chip placed on the glass carrier and the bond wires connecting the chip to the PCB.

Bond wire number	chip coordinates (x, y, z) [μm]	PCB coordinates (x, y, z) [μm]
1	$(80, 90, 900)$	$(80, -450, 0)$
2	$(220, 90, 900)$	$(220, -450, 0)$
3	$(360, 90, 900)$	$(360, -450, 0)$
4	$(500, 90, 900)$	$(500, -450, 0)$
5	$(640, 90, 900)$	$(640, -450, 0)$
6	$(780, 90, 900)$	$(780, -450, 0)$
7	$(920, 90, 900)$	$(920, -450, 0)$

Table 2.1: Points of attachment of the bond wires on the chip and on the PCB.

an uncertainty in the given value. The positions of the points of attachment of the bond wires on the chip and on the PCB, in the defined coordinate system, are presented in table 2.1. (The x- and y-coordinates on the PCB are only approximate and differ between modules.)

The chip and the glass carrier are placed on a PCB with width 35.6 mm and height 60.3 mm. The PCB is depicted in figure 2.4.

In figure 2.5, the entire gas sensor module can be seen. It consists of a black plastic house in which the PCB is placed. The gas enters through a filter on the top of the house through a diffusion process. There is a small plastic chimney with radius of 4 mm, that reaches from the top of the house down to the PCB, through which the gas moves down to the gas sensor component. The chimney is almost centered around the chip. The filter and the chimney prevent any strong winds from arising. There is only a small part of the PCB that is exposed to the gas from outside the module because of the chimney. The rest of the PCB is surrounded by air.

2.2 Material Properties

The chip is made of silicon on which there is a thin layer of silicon dioxide. On the upper surface of the chip there are aluminum layers for electrical connections and bond pads. Finally, there is another layer of silicon dioxide covering the electrical connections. The bond wires are made of gold and the glass carrier of pyrex. The PCB is a multilayer circuit board made of a resin filled glass fiber called FR4[1] and copper. The black house is fabricated from a polymer material called PBT[2] with 30% glass fiber.

[1] FR stands for "Flame Retardant" and type 4 indicates "woven glass reinforced epoxy resin" [1].

[2] PBT stands for "polybutylene terephthalate".

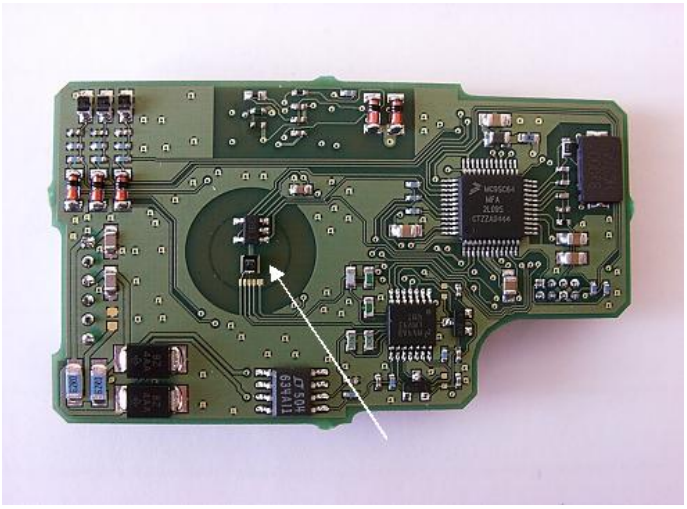

Figure 2.4: The chip and the glass carrier on the PCB, indicated by the arrow.

Figure 2.5: The gas sensor module.

Material	Density, ρ $[\frac{\text{kg}}{\text{m}^3}]$	Specific heat capacity, c_p $[\frac{\text{J}}{\text{kgK}}]$	Thermal conductivity, $\boldsymbol{k}$ $[\frac{\text{W}}{\text{mK}}]$
silicon [13]	$2.33 \cdot 10^3$	707	170
gold [13]	$19.32 \cdot 10^3$	129	311
copper [13]	$8.96 \cdot 10^3$	385	400
pyrex [9]	$2.25 \cdot 10^3$	860	1.34
FR4 [8]	$1.90 \cdot 10^3$	1200	0.23
PCB [8] [11]	$2.157 \cdot 10^3$	1117	$\begin{pmatrix} 18.5 & 0 & 0 \\ 0 & 18.5 & 0 \\ 0 & 0 & 0.25 \end{pmatrix}$

Table 2.2: Material properties.

In table 2.2, the material properties are listed[3]. All the materials except the PCB are assumed to be isotropic. The thermal conductivity of the PCB is therefore expressed by a matrix while all the other thermal conductivities are scalars. The material properties of the house are not listed as the house is not included in the sensor model, see section 2.6.

2.2.1 Thermal Conductivity of PCB

As stated above, the PCB is a multilayer circuit board made of a resin filled glass fiber called FR4 and copper. There are three layers of FR4 and four thin layers of copper. On the outer copper layers there are $4-6\mu$m thick nickel layers and 0.05μm thick gold layers. The PCB is finally covered by a green lacquer. In figure 2.6 the dimensions of the different layers are shown, except for the outer nickel, gold and lacquer layers.

The copper layers are perforated. At the two surface layers, the copper is intact at electrical connections and at groundings. The grounding is necessary for electrical reasons. The two inner layers are also perforated to a certain extent.

In the PCB, the copper and FR4 layers lie in the xy-plane. The thermal conductivity of the PCB in the xy-plane is different from the thermal conductivity in the z-direction. The properties follow the coordinate axes and the material is therefore called orthotropic, which is a special case of an anisotropic material where the properties do not have to follow the main coordinate axes. The

[3]The density is given for 300K and 0.1 MPa for silicon, gold and copper and for 293K and atmospheric pressure for pyrex. The specific heat capacity and the thermal conductivity are given for 300K for silicon, gold, copper and pyrex. (The specific heat capacity for pyrex is valid for the whole interval 273-573K.) It is not specified for which temperature or pressure the density, the specific heat capacity and the thermal conductivity of FR4 and the PCB are given.

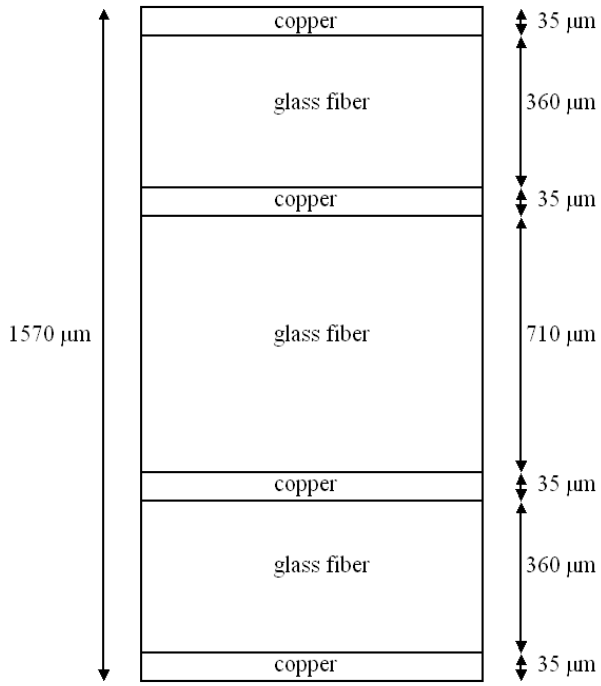

Figure 2.6: The cut away PCB.

thermal conductivity of an orthotropic material is expressed by the matrix

$$\boldsymbol{k} = \begin{pmatrix} k_{xx} & 0 & 0 \\ 0 & k_{yy} & 0 \\ 0 & 0 & k_{zz} \end{pmatrix} , \tag{2.1}$$

where only the diagonal elements are non zero [14].

The thermal conductivity in the xy-plane is expressed by $k_{xx} = k_{yy}$. The density and the specific heat capacity of the PCB as well as the thermal conductivity of the PCB in the xy-plane are computed using the online calculator found at [8]. To perform the calculation, the copper layers are specified by the number of layers, their thickness and their fill factor (a reduction factor that compensated for the copper layers not being homogeneous). The fill factor is assumed to be 10% for the outer layers and 95% for the inner layers. Furthermore, the total thickness of the PCB is specified.

To compute the thermal conductivity in the z-direction, k_{zz}, equation (2.2) is used [11].

$$\frac{\Delta}{k_{zz}} = \frac{\Delta_1}{k_1} + \cdots + \frac{\Delta_7}{k_7} \tag{2.2}$$

Δ is the total thickness of the PCB and k_{zz} is the thermal conductivity in the z-direction. Δ_i is the thickness and k_i is the thermal conductivity of the i'th layer.

2.2.2 Emissivity

To compute the amount of energy that is transferred from the surfaces to the gas due to radiation, the emissivity of the surface materials need to be determined. The outer layer of the chip consists mainly of silicon dioxide. The upside is covered with a layer of silicon dioxide while the silicon on the sides and on the underside have oxidized through a natural process. The glass carrier consists only of pyrex and the bond wires of gold. The PCB has a protecting layer of lacquer at the surface.

The values of the emissivity for pyrex, highly polished gold and black or white paint at certain temperature can be found in table 2.3.

The emissivity of silicon dioxide is assumed to be the value specified in table 2.4. Curves of the emissivity of silicon for different temperatures and different wavelengths are found in the literature. As oxides generally have higher values

Material	Emissivity, ϵ	Temperature, T [°C]
pyrex	0.9	400
gold, highly polished	0.018	226
paint, black or white	0.8	28

Table 2.3: Emissivity [18].

Material	Emissivity, ϵ
silicon dioxide	0.7
gold	0.04
lacquer	0.8

Table 2.4: Approximate values of emissivity.

of emissivity than the corresponding pure substances, the emissivity of silicon dioxide is assumed to be higher than the emissivity of silicon.

The emissivity of the gold in the bond wires is certainly higher than the value in table 2.3, as the gold is not highly polished. However, there are no other values of the emissivity of gold available in [18]. Through studying how much higher the emissivity is in [18] when other metals are "polished" instead of "highly polished", the emissivity of gold is approximated to the value in table 2.4.

The emissivity of the lacquer is not available. The lacquer has the appearance of green paint, and the emissivity is therefore approximated to the value of the emissivity of black or white paint in table 2.3.

The temperatures at which the emissivity is given do not correspond to the temperatures of the actual surfaces for which the emissivity is needed. However, these values are still used as they are the only ones available. There is a large uncertainty in the approximate values of the emissivity. The effect of this uncertainty is limited, as the radiative part of the heat transfer is small in comparison to the convective part, at least on the chip and the glass carrier which is shown in chapters 6 and 7.

2.3 Gas Properties

In the computation of the convection coefficient with the semi-empirical approach, formulas found in the literature are used, see section 6.1. These formulas include the following properties of the gas surrounding the sensor: the density, the specific heat capacity, the thermal conductivity and the viscosity. The gas is a mixture of air or nitrogen and hydrogen, which is further developed in section 2.4. Data for these properties are only available for each gas component. The properties of gas mixtures, when the properties of each component is known, have to be computed.

The amount of each gas component is specified in volume fraction. As shown in appendix A.1, mole and volume fractions are identical for ideal gases, which is assumed in this model. How to convert from volume to mass fraction is also described in appendix A.1.

In dry air there is approximately 78.09% nitrogen, 20.95% oxygen, 0.93% argon and 0.03% carbon dioxide measured in volume fractions [3]. To simplify the computations, the argon and carbon dioxide are neglected and it is assumed that air consists of 79% nitrogen and 21% oxygen.

The density, the specific heat capacity, the thermal conductivity and the viscosity of nitrogen, oxygen and hydrogen at different temperatures are accounted for in appendix A.2.

2.3.1 Properties of Gas Mixtures

First of all, the density of a gas mixture ρ_{mix}, is to be computed. This is possible if the density ρ_i and the volume fraction x_i^v of the pure gas components are known.

$$\rho_{mix} = \sum_i x_i^v \rho_i \tag{2.3}$$

The next step is to compute the specific heat capacity of a gas mixture, $c_{p,mix}$. If the specific heat capacity $c_{p,i}$ and the mass fraction x_i^m of the pure gas components are known, the specific heat capacity of the mixture is [9]:

$$c_{p,mix} = \sum_i x_i^m c_{p,i} \ . \tag{2.4}$$

This formula is valid for low-density gas mixtures, i.e. for gas mixtures at low pressures.

If the viscosity μ_i, the molar mass M_i and the mole fraction x_i^n of each pure component are known, the viscosity μ_{mix} of a gas mixture can be computed according to [4]:

$$\mu_{mix} = \sum_i \frac{x_i^n \mu_i}{\sum_j x_j^n \phi_{ij}} \ , \tag{2.5}$$

where

$$\phi_{ij} = \frac{[1 + (\mu_i/\mu_j)^{1/2}(M_j/M_i)^{1/4}]^2}{2\sqrt{2}(1 + M_i/M_j)^{1/2}} \ .$$

The equation is valid for gas mixtures at low pressures. It "has been extensively tested. [...] In most cases, only nonpolar mixtures were compared, and very good results obtained. For some systems containing hydrogen as one component, less satisfactory agreement was noted" [15, p.9.21-9.22]. It is therefore important to keep in mind that the calculations involving hydrogen might diverge from reality, especially for high concentrations of hydrogen.

Finally, the thermal conductivity k_{mix} of a gas mixture at the temperature T can be computed if the thermal conductivity k_i, the viscosity μ_i, the molar mass M_i, the normal boiling point T_{bi} and the mole fraction x_i^n for the pure components at the temperature T are known. The thermal conductivity for the mixture is then [4]:

$$k_{mix} = \sum_i \frac{k_i}{\sum_j (A_{ij} x_j^n / x_i^n)} \ , \tag{2.6}$$

where

$$\begin{aligned}
A_{ij} &= 1 \text{ for } i = j \ , \\
A_{ij} &= \frac{1}{4}\Big[1 + \sqrt{\Big(\frac{\mu_i}{\mu_j}\Big)\Big(\frac{M_j}{M_i}\Big)^{0.75}\Big(\frac{1 + S_i/T}{1 + S_j/T}\Big)}\Big]^2 \Big(\frac{1 + S_{ij}/T}{1 + S_j/T}\Big) \text{ for } i \neq j \ , \\
S_i &\approx 1.5 T_{bi} \text{ and} \\
S_{ij} &\approx 0.735 (S_i S_j)^{0.5} \ .
\end{aligned}$$

"The thermal conductivity of a mixture is much more sensitive to interaction effects than is the viscosity" [4, p.592]. It is therefore reasonable to expect the computation of the thermal conductivity to be less exact than the computation of the viscosity.

2.4 Parameter Range Definition

The range in which certain parameters are allowed to vary is determined. This is important to do, in order to know how the parameters can be varied in the simulations.

In table 2.5 the range for the temperature of the chip, T_{chip}, the temperature of the gas in the vicinity of the PCB, T_{gas}, and the power input to the heaters, $\dot{Q}_0$, are presented. The temperature of the chip is not varied in this diploma work, but kept constant at 140°C. However, the gas sensor module is developed to function for chip temperatures in the range given in table 2.5. The temperature of the gas far away from the sensor is specified to lie in the range −40°C to +125°C. The temperature of the gas in the vicinity of the PCB is assumed to be equal to the temperature far away from the sensor.

Parameter	Range
T_{chip}	$140 - 170$°C
T_{gas}	-40°C $- 125$°C
$\dot{Q}_0$	$0 - 800$ mW

Table 2.5: Parameter range for the chip temperature, the surrounding gas temperature and the power input to the heaters.

The volume fractions of the different gas components can vary between certain limits. There are two different gas modes. Air is mixed with hydrogen in the safe mode while nitrogen is mixed with hydrogen in the inert mode. To avoid the risk of explosion in the safe mode, there is a maximum allowed hydrogen concentration. In the inert mode on the other hand, there is no oxygen and therefore no risk of explosion. The hydrogen concentration can then take any value. The numbers are presented in table 2.6.

2.5 Assumptions and Simplifications

In order to obtain a model that can be solved using the available software and computer capacity, it is necessary to make certain assumptions and simplifications. Some of these have already been mentioned, but they are all summarized in this section.

When the difference in size between geometrical objects is large, the problem will be ill-conditioned and hard to solve using the FEM [17]. It is therefore best

Parameter	Range Safe mode	Range Inert mode
N_2	$75 - 79\%$	$0 - 100\%$
O_2	$20 - 21\%$	0
H_2	$0 - 4\%$	$0 - 100\%$

Table 2.6: Parameter range for nitrogen, oxygen and hydrogen gas in volume fraction.

not to include objects that are very thin or very small compared to the other objects in the model.

2.5.1 Limitation of Model

The gas surrounding the PCB can be considered as a separate domain in which the heat flow through convection is simulated. Another approach is to include the gas in the model through boundary conditions describing convection on the surfaces of the chip, the glass carrier and the PCB. The complexity of the problem will be significantly greater if the gas is considered as a separate domain than if it is included in the boundary conditions, which is why the latter approach is chosen. A consequence of this simplification is that the heating of the gas is neglected, i.e. the heat transferred from an object to the gas and back to an object is ignored.

The gas sensor module can be put in any direction, but the default orientation in the modeling procedure is horizontal with the chip on the upside of the PCB. In natural convection, the heat transfer from a surface depends on the direction of the gravitational force in relation to the surface, see section 1.3.2. Consequently, the values of the convection coefficient depend on the orientation of the gas sensor module.

2.5.2 Chip

The chip is considered as a block of pure silicon, i.e. the thin outer layers are not included in the model.

2.5.3 Heaters

The heaters are not represented by five three dimensional objects, but by one two dimensional rectangle constituting a boundary on the surface of the chip. The heat flow from the heaters is implicit in the specified temperature boundary condition of the rectangle, see section 3.3.1. The convection and radiation from the heaters are neglected as they cannot be included in a specified temperature boundary condition.

2.5.4 Bond Wires

The bond wires are not included as geometrical objects in the model as they are very thin. Instead, the points of attachment of the bond wires are represented by two dimensional boundaries through which a heat flow, calculated from the temperature difference of the points of attachment, is specified. Furthermore, the convection and radiation from the bond wires are neglected, which is motivated in section 3.4.1.

2.5.5 PCB

The PCB is modeled as a "flat" cylinder with the same height as the real PCB and radius 12 mm. This is a simplification as the real PCB is a block of significantly greater dimensions. However, to maintain a reasonable resolution of the meshing when using FEMLAB without getting too many degrees of freedom, it was decided that this was a necessary simplification.

The PCB is made of three layers of FR4 and four thin layers of copper. However, it is modeled as one solid block as thin objects make the problem difficult to solve. The outer nickel, gold and lacquer layers of the PCB are neglected.

When the temperature of the chip is raised, the PCB is heated to a certain extent. However, there are many other components that also contribute to the heating of the PCB. These contributions are neglected in the sensor model.

2.5.6 Material

All the materials except the PCB are assumed to be isotropic, i.e. the density, the specific heat capacity and the thermal conductivity are assumed not to vary with the temperature or with the spatial coordinates. The PCB on the other hand is orthotropic. The thermal conductivity is different in the xy-plane than in the z-direction, while the density and the specific heat capacity are assumed to be the same in all directions, see table 2.2.

The values of the emissivity of the surfaces are approximated in section 2.2.2.

2.5.7 Surrounding Gas

It is assumed that mole and volume fractions are the same for all gases in this model, see section 2.3. Air is supposed to be composed of 79% nitrogen and 21% oxygen.

The temperature of the gas in the vicinity of the PCB is approximated to be equal to the temperature far away from the sensor, as stated in section 2.4.

2.6 Sensor Model

When assumptions and simplifications are made, a model for the sensor system can be established.

2.6.1 Subdomains

The model includes the chip, the glass carrier and the PCB as three dimensional objects. These three objects are called subdomains. Heat transfer occurs by conduction in and between each subdomain. The conduction is described by the heat equation, which will be defined in section 3.2.

2.6.2 Boundaries

Each subdomain is bounded by two dimensional surfaces. All surfaces are described by boundary conditions to the heat equation, defined in section 3.4.

The heaters are represented by a two dimensional rectangle on the upper surface of the chip, on which a temperature is defined. Heat transfer occurs by an inward heat flow representing the power input. The points of attachment of the bond wires are modeled by two dimensional circular surfaces on the chip and on the PCB, through which a heat flow representing conduction in the bond wires can be defined. The envelope surface of the cylinder representing the PCB is looked upon as being insulated. Heat transfer occurs by convection and radiation on all other surfaces.

The upper surface of the PCB is divided into two parts; an inner circle representing the chimney and an outer segment. The surrounding gas is air on the outer segment and on the underside of the PCB, while it consists of air or nitrogen mixed with hydrogen on all other surfaces.

The geometrical model can be seen in figure 2.7. A close-up of the chip and the glass carrier is shown is figure 2.8.

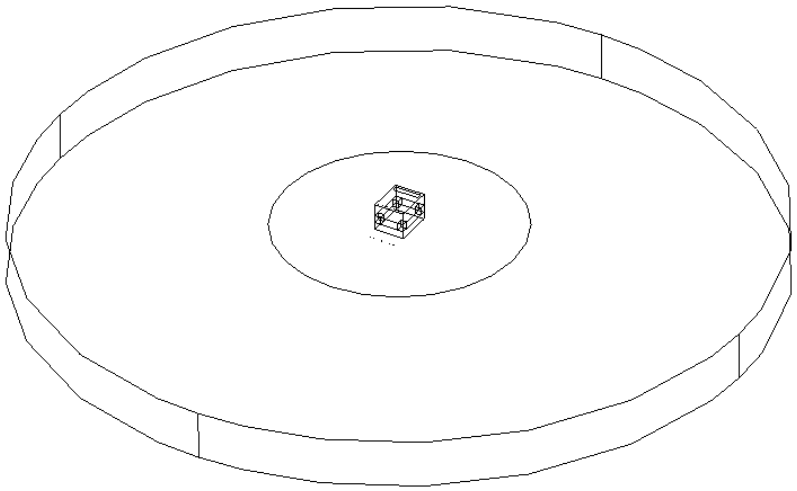

Figure 2.7: The geometrical model.

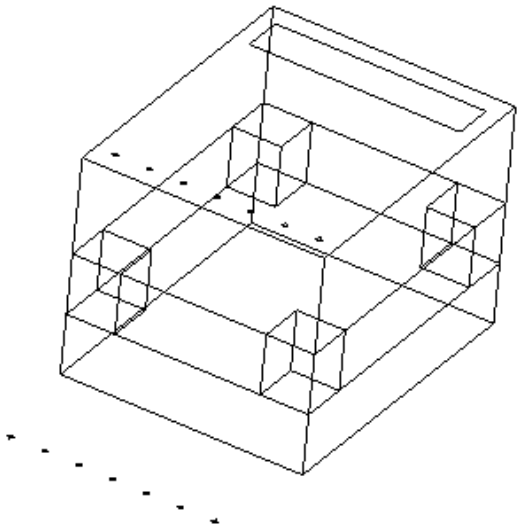

Figure 2.8: A close-up of the chip and the glass carrier in the geometrical model.

Chapter 3

Heat Equation and Boundary Conditions

In this chapter, the equation describing conduction in a domain in general, and in the subdomains of the sensor model in particular, is defined. Furthermore, all possible boundary conditions are accounted for and the boundary conditions for the sensor model are decided.

3.1 Heat Equation

The heat flow in the chip, the glass carrier, the bond wires and the PCB is a mechanism of conduction, which can be described by the heat equation [5]:

$$\rho c_p \frac{\partial T}{\partial t} - \nabla \cdot (\boldsymbol{k} \nabla T) - \dot{g} = 0 \ , \tag{3.1}$$

where T is the temperature, ρ is the density, c_p is the specific heat capacity at constant pressure, $\boldsymbol{k}$ is the thermal conductivity and $\dot{g}$ is the rate of heat generation per unit of volume ($\mathrm{W/m^3}$).

3.2 Heat Equation for Sensor Model

The heat equation (3.1) defines the conduction in the three different subdomains: the chip, the glass carrier and the PCB. The equation is solved for steady-state conditions and therefore $\partial T/\partial t = 0$. The thermal conductivity is assumed not to vary along the main coordinate axes and the equation simplifies to

$$\boldsymbol{k} \nabla^2 T + \dot{g} = 0 \ . \tag{3.2}$$

The rate of heat generation, $\dot{g}$, is nonzero only for the heaters. However, the heaters are not represented by geometrical objects, but included in the boundary conditions as described in section 2.5.4. The equation to be solved in each subdomain is therefore

$$\boldsymbol{k} \nabla^2 T = 0 \ . \tag{3.3}$$

The chip and the glass carrier are made of isotropic materials, meaning that the thermal conductivity $\boldsymbol{k}$ is expressed by a diagonal matrix with the scalar k in the diagonal. Equation (3.3) therefore simplifies to:

$$\frac{\partial^2 T}{\partial x^2} + \frac{\partial^2 T}{\partial y^2} + \frac{\partial^2 T}{\partial z^2} = 0 \ . \tag{3.4}$$

The PCB on the other hand, consists of an orthotropic material where the thermal conductivity is expressed by the matrix in equation (2.1), and equation (3.3) becomes:

$$k_{xx}\frac{\partial^2 T}{\partial x^2} + k_{yy}\frac{\partial^2 T}{\partial y^2} + k_{zz}\frac{\partial^2 T}{\partial z^2} = 0 \ . \tag{3.5}$$

Equations (3.4) and (3.5) are PDEs that are solved with the boundary conditions described in section 3.4.

3.3 Boundary Conditions

There are five different types of boundary conditions on domains described by the heat equation (3.1): specified temperature, specified heat flow, convection, radiation and generalized boundary conditions [5]. Specified temperature is a Dirichlet boundary condition[1], while all the others are Neumann boundary conditions[2].

When deriving the Neumann boundary conditions, Fourier's law described in equation (1.1) is needed. The heat flow that exits the surface of a domain is the normal component of the heat flow in Fourier's law:

$$-\boldsymbol{n} \cdot (\boldsymbol{k}\nabla T) = \boldsymbol{n} \cdot \dot{\boldsymbol{q}} \ , \tag{3.6}$$

where $\boldsymbol{n}$ is the normal vector to the surface and $\dot{\boldsymbol{q}}$ is a vector representing the heat flow per unit of area. The equation can be rewritten as:

$$\boldsymbol{n} \cdot (\boldsymbol{k}\nabla T) = -\dot{q} \ , \tag{3.7}$$

where $\dot{q}$ is the normal component of $\dot{\boldsymbol{q}}$.

3.3.1 Specified Temperature Boundary Condition

If the temperature on a boundary is known to be $T_0(x, y, z)$, the boundary condition can be specified through:

$$T = T_0(x, y, z) \ . \tag{3.8}$$

On the surface representing the heaters, the specified temperature boundary condition will be used with $T_0 = T_{chip}$.

[1] In a Dirichlet boundary condition, the temperature is specified.

[2] In a Neumann boundary condition, one of the derivatives of the temperature is set. In this context the normal heat flux is specified, which implies defining the derivative of the temperature in the normal direction.

3.3.2 Specified Heat Flow Boundary Condition

A boundary condition can specify the heat flow entering the surface in question. If $\dot{q}_0$ designates the inward heat flow, $\dot{q} = -\dot{q}_0$ in equation (3.7) and the boundary condition becomes:

$$\boldsymbol{n} \cdot (\boldsymbol{k}\nabla T) = \dot{q}_0 \ . \tag{3.9}$$

An insulated boundary can be considered as a special case of a specified heat flow boundary condition, with no heat flow exiting or entering the surface.

$$\boldsymbol{n} \cdot (\boldsymbol{k}\nabla T) = 0 \tag{3.10}$$

3.3.3 Convection Boundary Condition

The heat flow exiting the surface due to convection, $\dot{q}_{convection}$, can be put equal to $\dot{q}$ in equation (3.7). The boundary condition is then:

$$\boldsymbol{n} \cdot (\boldsymbol{k}\nabla T) = -\dot{q}_{convection} \ . \tag{3.11}$$

The contribution of convection at a boundary is expressed by Newton's law of cooling, equation (1.3), which is inserted into equation (3.11):

$$\boldsymbol{n} \cdot (\boldsymbol{k}\nabla T) = h(T_{gas} - T) \ . \tag{3.12}$$

There is a heat flow due to convection at all surfaces of the sensor system. The convection coefficient depends on the temperatures of the surface and the gas surrounding the sensor, on the gas composition and on the geometry. In particular, the convection coefficient, and consequently the heat flow, grows with the concentration of hydrogen gas. How to compute the convection coefficient is described in section 6.1.

3.3.4 Radiation Boundary Condition

The heat flow $\dot{q}_{radiation}$ exits the surface due to radiation, and by putting it equal to $\dot{q}$ in equation (3.7), the boundary condition becomes:

$$\boldsymbol{n} \cdot (\boldsymbol{k}\nabla T) = -\dot{q}_{radiation} \ . \tag{3.13}$$

The contribution of radiation at a boundary is expressed by equation (1.4), giving:

$$\boldsymbol{n} \cdot (\boldsymbol{k}\nabla T) = \epsilon\sigma(T_{ambient}^4 - T^4) \ . \tag{3.14}$$

Apart from convection, radiation also occurs at all surfaces of the sensor system, although this contribution is smaller.

3.3.5 Generalized Boundary Condition

At a surface, both convection and radiation can occur simultaneously. The boundary condition is then:

$$\boldsymbol{n} \cdot (\boldsymbol{k}\nabla T) = h(T_{gas} - T) + \epsilon\sigma(T_{ambient}^4 - T^4) \ . \tag{3.15}$$

As there are both convection and radiation at all surfaces of the sensor system, this boundary condition will be frequently used.

A boundary condition specifying an inward heat flow q_0, apart from the convection and radiation, is defined by:

$$\boldsymbol{n} \cdot (\boldsymbol{k}\nabla T) = q_0 + h(T_{gas} - T) + \epsilon\sigma(T_{ambient}^4 - T^4) \ . \tag{3.16}$$

3.4 Boundary Conditions for Sensor Model

The boundary conditions for the sensor model can now be defined. The envelope surface of the PCB is insulated, specified by boundary condition (3.10). At the heaters, there is a specified temperature boundary condition, defined in equation (3.8). The boundary conditions at the points of attachment of the bond wires define the conduction in the bond wires, and these are developed in section 3.4.1. At all other surfaces, the boundary conditions are given by the generalized boundary condition (3.15) including convection and radiation. A list of all the boundary conditions of the sensor model is given below.

1. Envelope surface of PCB (insulation):

$$\boldsymbol{n} \cdot (\boldsymbol{k}\nabla T) = 0 \tag{3.17}$$

2. Heaters (temperature):

$$T = T_{chip} \tag{3.18}$$

3. Point of attachment of bond wire m on chip (conduction):

$$\boldsymbol{n} \cdot (\boldsymbol{k}\nabla T) = -\frac{k_{gold}}{L}(T - T_{PCB,m}) \tag{3.19}$$

4. Point of attachment of bond wire m on PCB (conduction):

$$\boldsymbol{n} \cdot (\boldsymbol{k}\nabla T) = \frac{k_{gold}}{L}(T_{chip,m} - T) \tag{3.20}$$

5. All other surfaces (convection and radiation):

$$\boldsymbol{n} \cdot (\boldsymbol{k}\nabla T) = h(T_{gas} - T) + \epsilon\sigma(T_{ambient}^4 - T^4) \tag{3.21}$$

3.4.1 Boundary Conditions for Points of Attachment of Bond Wires

The heat flow in the bond wires is described by conduction. As mentioned in section 2.5.4, the points of attachment of the bond wires are represented by two dimensional boundaries, into or out of which a heat flow corresponding to the conduction is specified. The convection and radiation from the surfaces of the bond wires are neglected.

The bond wires are assumed to be straight rods with length L, through which heat flows from a higher to a lower temperature. The heat flow in a rod can be described by [13]:

$$\dot{q} = -k\frac{dT}{dx} \ , \tag{3.22}$$

where $\dot{q}$ is the rate of heat flow per unit of area, k is the thermal conductivity and dT/dx is the change in temperature along the rod.

As the heat convection and radiation are neglected, the heat flow across the bond wire is constant, i.e. the heat that enters a bond wire at $x = 0$ exits the bond wire at $x = L$. Using this assumption, the temperature decreases linearly and the equation can be written as:

$$\dot{q}_{bondwire} = \frac{k_{gold}}{L}(T_{chip} - T_{PCB}) \ , \tag{3.23}$$

where T_{chip} is the temperature at the point of attachment of the bond wire on the chip and T_{PCB} is the temperature at the point of attachment of the bond wire on the PCB.

First, the boundary conditions for the points of attachment on the chip will be defined. $\dot{q}_{bondwire}$ designates the outward heat flow from the chip. $\dot{q} = \dot{q}_{bondwire}$ in equation (3.7) gives:

$$\boldsymbol{n} \cdot (\boldsymbol{k}\nabla T) = -\dot{q}_{bondwire} \ . \tag{3.24}$$

Inserting equation (3.23) into this equation gives the boundary condition for the point of attachment of bond wire m on the chip:

$$\boldsymbol{n} \cdot (\boldsymbol{k}\nabla T) = -\frac{k_{gold}}{L}(T - T_{PCB,m}) \ , \tag{3.25}$$

where $T_{PCB,m}$ is the temperature at the point of attachment of bond wire m on the PCB.

Next, the boundary conditions for the points of attachment on the PCB are specified. $\dot{q}_{bondwire}$ designates the heat flow into the PCB. $\dot{q} = -\dot{q}_{bondwire}$ in equation (3.7) gives:

$$\boldsymbol{n} \cdot (\boldsymbol{k}\nabla T) = \dot{q}_{bondwire} \ . \tag{3.26}$$

The boundary condition for the point of attachment of bond wire m on the PCB is then:

$$\boldsymbol{n} \cdot (\boldsymbol{k}\nabla T) = \frac{k_{gold}}{L}(T_{chip,m} - T) \ , \tag{3.27}$$

where $T_{chip,m}$ is the temperature at the point of attachment of bond wire m on the chip.

Motivation of Convection and Radiation Negligence in Bond Wires

In reality, some of the heat flow that enters the bond wires exits the surfaces of the bond wires through convection and radiation. To motivate this negligence, approximate values of the heat flow through convection and radiation will be computed and compared to an approximate value of the heat flow through conduction.

The bond wires are considered as straight vertical rods. The temperature of the bond wires is assumed to decrease from $T_{chip} = 413$ K to $T_{PCB} = 313$ K. The temperature of the surrounding gas is supposed to be $T_{gas} = 300$ K, the same as the temperature of the surface of the house enclosing the PCB, $T_{ambient}$. The length L and the radius r of the bond wires can be found in section 2.1.

The convection heat flow is calculated according to equation (1.3). The temperature of the bond wires is computed as their mean value; $T_{rod} = (T_{chip} + T_{PCB})/2 = 363$ K. The convection coefficient is calculated assuming that the bond wires are vertical cylinders with small diameters, which is described in appendix B. In air, $h_{air} = 20$ W/m^{2}K and in hydrogen, $h_{H_2} = 52$ W/m^{2}K. These values give an indication of the size of the convection coefficient, but it is important to keep in mind the uncertainty in the computation. To obtain an upper limit for the heat flow through convection, the convection coefficient for hydrogen is used. The heat flow per unit of area for one bond wire is then:

$$\dot{q}_{convection} = h_{H_2}(T_{rod} - T_{gas}) \ . \tag{3.28}$$

The total heat flow can be obtained as the area of the envelope surface of the bond wires is known.

$$\begin{aligned} \dot{Q}_{convection} &= A_{envelope} h_{H_2}(T_{rod} - T_{gas}) \\ &= 2\pi r L h_{H_2}(T_{rod} - T_{gas}) \\ &\approx 0.4 \text{ mW} \end{aligned} \tag{3.29}$$

The next step is to compute the heat flow through radiation using equation (1.5). The Stefan-Boltzmann constant σ is $5.67 \cdot 10^{-8}$ W/m^{2}K^4 [13]. The value of the emissivity ϵ for gold can be found in table 2.4.

$$\dot{q}_{radiation} = \epsilon\sigma(T_{rod}^4 - T_{ambient}^4) \tag{3.30}$$

As for the convection, the area needed is the envelope surface of the bond wires, which gives:

$$\begin{aligned} \dot{Q}_{radiation} &= A_{envelope}\epsilon\sigma(T_{rod}^4 - T_{ambient}^4) \\ &= 2\pi r L \epsilon_{gold}\sigma(T_{rod}^4 - T_{ambient}^4) \\ &\approx 0.003 \text{ mW} \ . \end{aligned} \tag{3.31}$$

Finally, the conduction heat flow can be computed using equation (3.23), provided that the convection and radiation are neglected. The thermal conductivity of gold can be found in section 2.2.

$$\dot{q}_{conduction} = \frac{k_{gold}}{L}(T_{chip} - T_{PCB}) \tag{3.32}$$

The cross section area of the bond wires can be computed, which gives the total heat conduction through one bond wire:

$$\begin{aligned} \dot{Q}_{conduction} &= \frac{k_{gold}A}{L}(T_{chip} - T_{PCB}) \\ &= \frac{k_{gold}\pi r^2}{L}(T_{chip} - T_{PCB}) \\ &\approx 10 \text{ mW} \ . \end{aligned} \tag{3.33}$$

It is clear that the convection and radiation contributions to the heat flow in the bond wires are small in comparison to the conduction. It is therefore a reasonable simplification to neglect the convection and radiation from the surfaces of the bond wires.

Chapter 4

Finite Element Method

The aim of the finite element method, used in the software FEMLAB, is to solve partial differential equations with boundary conditions by an approximate method. The idea is to divide the geometric domain into so called finite elements, and to approximate the unknown function by a simple function on each element. One way to obtain higher accuracy is to increase the number of finite elements. The ideas and basic concepts of the method are presented in this chapter. The presentation is adapted from [14] and [16].

4.1 2D Stationary Heat Transfer Problem

To simplify the presentation, a two dimensional stationary heat transfer problem with linear boundary conditions will be analyzed.

Consider an area A consisting of an orthotropic material with the thermal conductivity

$$\boldsymbol{k} = \begin{pmatrix} k_{xx} & 0 \\ 0 & k_{yy} \end{pmatrix} , \tag{4.1}$$

and an heat source generating the heat $\dot{g}$. The area is surrounded by a gas with the temperature T_{gas}. The boundary L is divided into the two parts L_1 and L_2, where the boundary condition on L_1 is specified by an inward heat flow $\dot{q}_0$ and the boundary condition on L_2 by convection with the convection coefficient h. Figure 4.1 shows area A bounded by L_1 and L_2.

4.2 Strong Form

The heat equation (3.1) with $\partial T/\partial t = 0$ describes the conduction in the region. The specified heat flow boundary condition is expressed by equation (3.9) and the convection boundary condition by equation (3.12). The so called strong

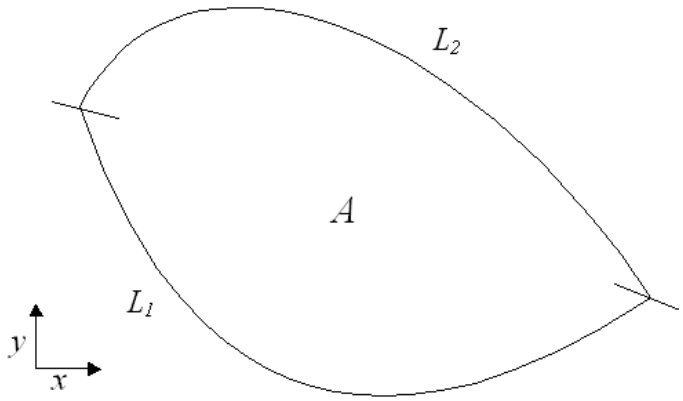

Figure 4.1: The area A bounded by L_1 and L_2.

form of the problem can then be formulated as

$$\begin{aligned} \nabla \cdot (\boldsymbol{k}\nabla T) + \dot{g} &= 0 && (4.2)\\ \boldsymbol{n} \cdot (\boldsymbol{k}\nabla T) &= \dot{q}_0 \text{ on } L_1 && (4.3)\\ \boldsymbol{n} \cdot (\boldsymbol{k}\nabla T) &= h(T_{gas} - T) \text{ on } L_2\ . && (4.4) \end{aligned}$$

4.3 Weak Form

The starting point for the FEM is the so called weak form of the partial differential equation and its boundary conditions. The weak form is derived from the strong form, starting with the PDE without boundary conditions.

$$\nabla \cdot (\boldsymbol{k}\nabla T) + \dot{g} = 0 \tag{4.5}$$

The equation is multiplied by an arbitrary test function $v(x, y)$ and integrated over the area A.

$$\int_A [v\nabla \cdot (\boldsymbol{k}\nabla T) + v\dot{g}]dA = 0 \tag{4.6}$$

Partial integration and the use of Stokes' theorem give the result below.

$$\oint_L v(\boldsymbol{k}\nabla T) \cdot \boldsymbol{n}dL - \int_A \nabla v \cdot (\boldsymbol{k}\nabla T)dA + \int_A v\dot{g}dA = 0 \tag{4.7}$$

The formula is rearranged so that the area integrals are on the left hand side and the line integral on the right hand side.

$$\int_A [\nabla v \cdot (\boldsymbol{k}\nabla T) - v\dot{g}]dA = \oint_L v(\boldsymbol{k}\nabla T) \cdot \boldsymbol{n}dL \tag{4.8}$$

The boundary conditions (4.3) and (4.4) are now inserted into equation (4.8), which gives the weak form.

$$\int_A [\nabla v \cdot (\boldsymbol{k}\nabla T) - v\dot{g}]dA = \int_{L1} v\dot{q}_0 dL + \int_{L2} vh(T_{gas} - T)dL \tag{4.9}$$

There are several advantages when using the weak form compared to the strong form, which is why the weak form is chosen as the starting point for the FEM.

As already mentioned, the unknown function T is approximated by simple functions on finite elements. A very important advantage with using the weak form, is that the approximate function needs only to be once differentiable. If the strong form would be used, the approximate function would have to be twice differentiable. The weak form is applicable even when discontinuities occur, which also favors this form. In the context of the sensor model, discontinuities of material properties can be mentioned as an example. The strong form needs to be modified to be valid for discontinuities [14].

4.4 Meshing

The process of dividing the geometry into finite elements is called meshing. In two dimensions, the mesh elements can be triangles or rectangles. Triangles are chosen for area A, and an example of a mesh is shown in figure 4.2. The corners of an element are called nodes, see figure 4.3. The nodes are numbered from 1 to n.

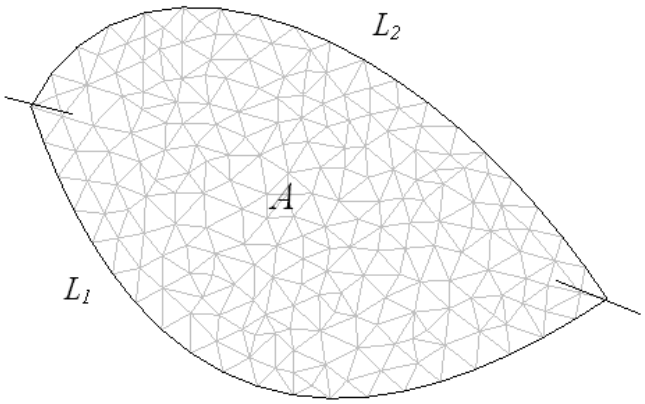

Figure 4.2: The meshing of area A.

The unknown function T will be approximated by a simple function on each element. In order to obtain a more exact solution, the region can be divided into smaller elements.

4.5 Approximating Function

The unknown function T is approximated by T^{app}:

$$T(x, y) \approx T^{app}(x, y) = \boldsymbol{N}(x, y)\boldsymbol{a} \ , \tag{4.10}$$

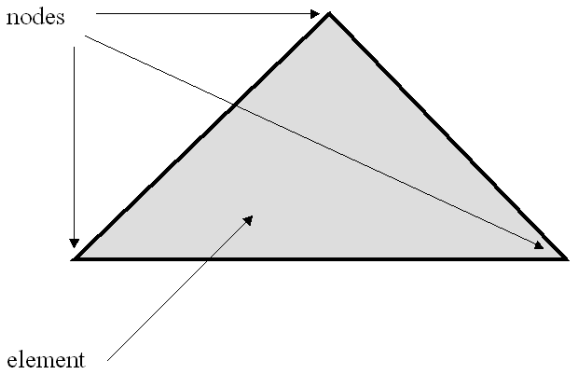

Figure 4.3: An element and its nodes.

where

$$\boldsymbol{N}(x,y) = \begin{pmatrix} N_1(x,y) & \cdots & N_n(x,y) \end{pmatrix}, \qquad \boldsymbol{a} = \begin{pmatrix} T_1 \\ \vdots \\ T_n \end{pmatrix}.$$

N_i is called a basis function and T_i is an unknown parameter, for $i = 1, \ldots, n$. The basis function N_i is local and nonzero only for the elements adjacent to node i, see figure 4.4. The part of the basis function corresponding to an element is

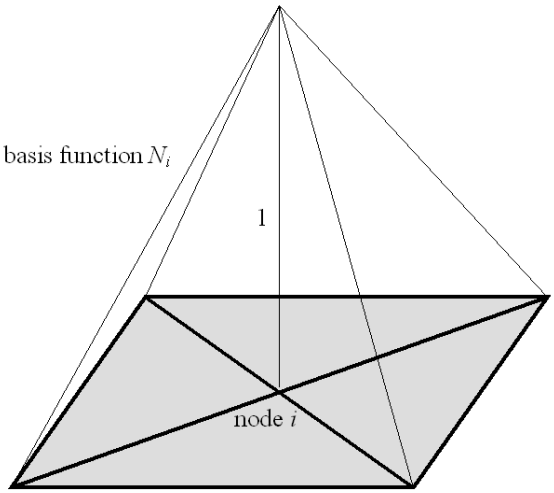

Figure 4.4: Basis function N_i corresponding to node i.

called element function, i.e. the basis function in figure 4.4 is composed of four element functions. The value of the basis function N_i at node i is 1. The element

functions can be polynomial or trigonometric functions. It is common to choose polynomial functions, and in this presentation we use linear polynomials.

$T^{app}(x_i, y_i)$ gives an approximate value of the temperature at node i, where (x_i, y_i) are the coordinates of node i.

$$\begin{aligned} T^{app}(x_i, y_i) &= \boldsymbol{N}(x_i, y_i)\boldsymbol{a} \\ &= \begin{pmatrix} N_1(x_i, y_i) & \cdots & N_i(x_i, y_i) & \cdots & N_n(x_i, y_i) \end{pmatrix} \begin{pmatrix} T_1 \\ \vdots \\ T_i \\ \vdots \\ T_n \end{pmatrix} \\ &= \begin{pmatrix} 0 & \cdots & 1 & \cdots & 0 \end{pmatrix} \begin{pmatrix} T_1 \\ \vdots \\ T_i \\ \vdots \\ T_n \end{pmatrix} \\ &= T_i \ . \end{aligned} \tag{4.11}$$

Accordingly, the unknown parameter T_i is the approximate temperature at node i.

Linear polynomials could not be used if the strong form of the problem would be the starting point for the method, as second order derivates for linear functions are zero. When using the weak form, linear polynomials do not cause any problems.

4.6 Test Function

The test function is an arbitrary function and can be chosen in many different ways. It can be expressed as

$$v(x, y) = \boldsymbol{V}(x, y)\boldsymbol{c} \ , \tag{4.12}$$

where

$$\boldsymbol{V}(x, y) = \begin{pmatrix} V_1(x, y) & \cdots & V_n(x, y) \end{pmatrix} \ , \qquad \boldsymbol{c} = \begin{pmatrix} c_1 \\ c_2 \\ \vdots \\ c_n \end{pmatrix} \ .$$

The functions V_i are specified when choosing the test function while c_i are unknown, arbitrary parameters. (The test function is arbitrary and the functions V_i are decided, which means that the parameters c_i must be arbitrary.)

"It turns out that a particularly suitable choice of the test function in the FE method is obtained by the *Galerkin method* (Galerkin, 1915) which is also used in other formulations than the FE approach. More generally, the Galerkin

method is an example of a so-called *weighted residual method*" [14, p.142-143]. In the Galerkin method, the functions V_i are chosen equal to the basis functions N_i and $v(x, y)$ can be expressed as:

$$v(x, y) = \boldsymbol{N}(x, y)\boldsymbol{c} \ . \tag{4.13}$$

4.7 Formulation of the Finite Element Method

The weak form (4.9) with $T \approx T^{app}$ is:

$$\int_A \nabla v \cdot (\boldsymbol{k}\nabla T^{app})dA = \int_{L1} v\dot{q}_0 dL + \int_{L2} vh(T_{gas} - T^{app})dL + \int_A v\dot{g}dA \ . \tag{4.14}$$

This is the starting point for the formulation of the FEM. In this form, the gradient of the temperature is needed. The gradient of T^{app} is:

$$\nabla T^{app} = \nabla(\boldsymbol{N}\boldsymbol{a}) = (\nabla \boldsymbol{N})\boldsymbol{a} = \boldsymbol{B}\boldsymbol{a} \ , \tag{4.15}$$

as the vector $\boldsymbol{a}$ does not depend on x and y and where

$$\boldsymbol{B} = \nabla N = \begin{pmatrix} \frac{\partial N_1}{\partial x} & \frac{\partial N_2}{\partial x} & \dots & \frac{\partial N_n}{\partial x} \\ \frac{\partial N_1}{\partial y} & \frac{\partial N_2}{\partial y} & \dots & \frac{\partial N_n}{\partial y} \end{pmatrix} \ . \tag{4.16}$$

Equations (4.15) and (4.10) are inserted into the weak form (4.14):

$$\int_A \nabla v \cdot (\boldsymbol{k}\boldsymbol{B}\boldsymbol{a})dA = \int_{L1} v\dot{q}_0 dL + \int_{L2} vh(T_{gas} - \boldsymbol{N}\boldsymbol{a})dL + \int_A v\dot{g}dA \ , \tag{4.17}$$

which can be rearranged as:

$$\int_A (\nabla v)^T \boldsymbol{k}\boldsymbol{B}\boldsymbol{a}dA + \int_{L2} vh\boldsymbol{N}\boldsymbol{a}dL = \int_{L1} v\dot{q}_0 dL + \int_{L2} vhT_{gas}dL + \int_A v\dot{g}dA \ . \tag{4.18}$$

v is chosen according to equation (4.13), and the gradient of v is then:

$$\nabla v = \nabla(\boldsymbol{N}\boldsymbol{c}) = (\nabla \boldsymbol{N})\boldsymbol{c} = \boldsymbol{B}\boldsymbol{c} \ . \tag{4.19}$$

v is equivalent to $v^T = \boldsymbol{c}^T\boldsymbol{N}^T$. v^T and ∇v are inserted into the weak form:

$$\begin{aligned} \int_A (\boldsymbol{B}\boldsymbol{c})^T \boldsymbol{k}\boldsymbol{B}\boldsymbol{a}dA \ &+ \ \int_{L2} \boldsymbol{c}^T\boldsymbol{N}^T h\boldsymbol{N}\boldsymbol{a}dL \\ &= \ \int_{L1} \boldsymbol{c}^T\boldsymbol{N}^T\dot{q}_0 dL + \int_{L2} \boldsymbol{c}^T\boldsymbol{N}^T hT_{gas}dL + \int_A \boldsymbol{c}^T\boldsymbol{N}^T\dot{g}dA \ . \end{aligned} \tag{4.20}$$

$\boldsymbol{c}^T$ is extracted from the integrals, giving:

$$\begin{aligned} \boldsymbol{c}^T\Big(\int_A \boldsymbol{B}^T\boldsymbol{k}\boldsymbol{B}\boldsymbol{a}dA \ &+ \ \int_{L2} h\boldsymbol{N}^T\boldsymbol{N}\boldsymbol{a}dL\Big) \\ &= \ \boldsymbol{c}^T\Big(\int_{L1} \boldsymbol{N}^T\dot{q}_0 dL + \int_{L2} \boldsymbol{N}^T hT_{gas}dL + \int_A \boldsymbol{N}^T\dot{g}dA\Big) \ . \end{aligned} \tag{4.21}$$

As $\boldsymbol{c}$ can be chosen arbitrarily, the equation can be simplified further.

$$(\int_A \boldsymbol{B}^T \boldsymbol{k} \boldsymbol{B} dA + \int_{L2} h \boldsymbol{N}^T \boldsymbol{N} dL)\boldsymbol{a} = \int_{L1} \boldsymbol{N}^T \dot{q}_0 dL + \int_{L2} \boldsymbol{N}^T h T_{gas} dL + \int_A \boldsymbol{N}^T \dot{g} dA \tag{4.22}$$

The expression can be written in a more compact form if we use the following notation:

$$\begin{aligned} \boldsymbol{K} &= \int_A \boldsymbol{B}^T \boldsymbol{k} \boldsymbol{B} dA + \int_{L2} h \boldsymbol{N}^T \boldsymbol{N} dL \\ \boldsymbol{f} &= \int_{L1} \boldsymbol{N}^T \dot{q}_0 dL + \int_{L2} \boldsymbol{N}^T h T_{gas} dL + \int_A \boldsymbol{N}^T \dot{g} dA \ . \end{aligned} \tag{4.23}$$

$\boldsymbol{K}$ is called the stiffness matrix and $\boldsymbol{f}$ the force vector. The equation is then

$$\boldsymbol{K}\boldsymbol{a} = \boldsymbol{f} \ , \tag{4.24}$$

which is a system of linear equations.

The stiffness matrix $\boldsymbol{K}$ is an $n \times n$-matrix where element (i, j) is:

$$K_{ij} = \int_A (k_{xx} \frac{\partial N_i}{\partial x} \frac{\partial N_j}{\partial x} + k_{yy} \frac{\partial N_i}{\partial y} \frac{\partial N_j}{\partial y}) dA + \int_{L2} h N_i N_j dL \ . \tag{4.25}$$

The basis function N_i is non-zero only for elements containing node i. Consequently, K_{ij} is non-zero only for elements containing both node i and node j. The stiffness matrix will therefore be a sparse matrix, containing zeros in the majority of the elements. The system of linear equations can be solved by gaussian elimination. For large systems, it is important to use methods taking advantage of the sparsity of the matrix.

The unknown vector $\boldsymbol{a}$, containing the temperatures at the nodes, is obtained when solving the system of linear equations. Temperatures at arbitrary points can then be found by the use of

$$T^{app} = \boldsymbol{N}\boldsymbol{a} \ . \tag{4.26}$$

The heat flow at an arbitrary point can be obtained through the use of Fourier's law below.

$$\boldsymbol{q} = -\boldsymbol{k} \nabla T^{app} = -\boldsymbol{k}\boldsymbol{B}\boldsymbol{a} \tag{4.27}$$

An approximate solution of the PDE with the corresponding boundary conditions is obtained through this finite element method. To get a more exact solution, the number of mesh elements can be increased and the system solved once again.

Chapter 5

Experiments

The experimental setup and plan are presented in this chapter. The aim of the experiments is to measure the power input to the heaters needed to maintain the constant chip temperature $140°\mathrm{C}$, for different hydrogen concentrations and different temperatures of the surrounding gas. The parameters from which the power input is calculated are described. Finally, the experimental data is accounted for. The execution of the experiments are performed in cooperation with engineers at AppliedSensor.

5.1 Experimental Setup

The gas sensor house used in the experiments is a prototype, as the real houses are not yet produced when the majority of the experiments are performed. The prototype is made of polyamide and glass fiber, a white and light material, different from the black plastic material of the real houses. In all the experiments accounted for, the gas sensor module called A2012 is used.

The gas sensor module can be put in an oven or in a climate chamber, where the surrounding gas temperature can be varied. When the temperature of the gas is changed, the temperature of the whole module is affected. In the oven, it is only possible to obtain temperatures above room temperature, while all temperatures in the parameter range of T_{gas}, see section 2.4, can be reached in the climate chamber. Unfortunately, the access to the climate chamber was limited. All experiments accounted for are therefore performed in the oven.

A gas mixing system is used to obtain a mixture of nitrogen or air and hydrogen, see figure 5.1. A gas block, through which the gas reaches the sensor chip, is put on top of the gas sensor module. The gas flows continuously into and out of the gas block through flexible tubes. The hydrogen mixture is limited to the gas block, the chimney and the tubes. The rest of the oven is filled with air. Data from the sensor is stored on a local computer, using the electrical interface from the sensor module. In figure 5.2, the set-up in the oven can be seen.

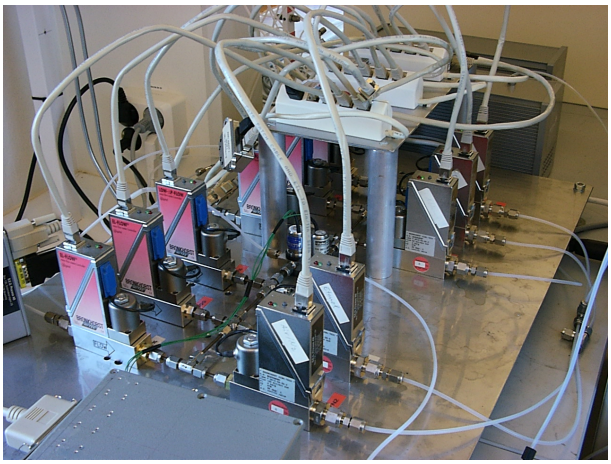

Figure 5.1: The gas mixing system.

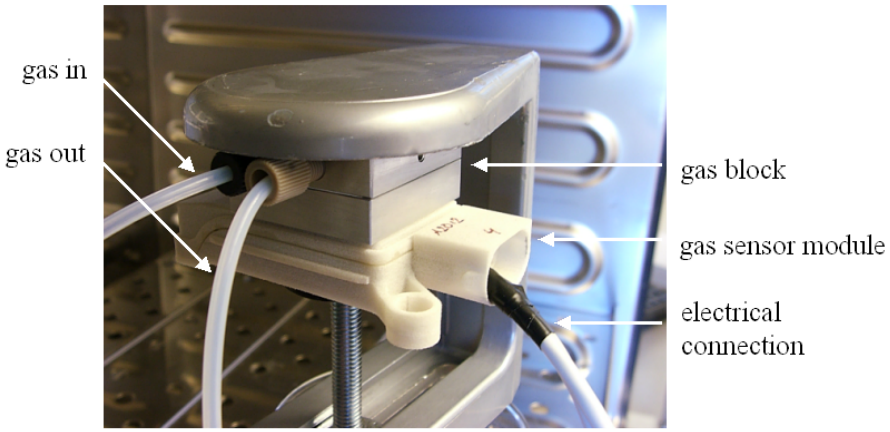

Figure 5.2: The gas sensor module and the gas block in the oven.

5.2 Experimental Plan

The experimental plan describes how the composition and temperature of the gas reaching the sensor chip are varied.

All gas concentrations specified in section 2.4 can be obtained. However, it is decided only to do experiments in the inert mode, where hydrogen is mixed with nitrogen. The reason is that a greater range of hydrogen concentrations can be reached in the inert mode than in the safe mode. The concentration of hydrogen is varied from 0 to 100% in steps of 4%. The regulators are not specified to adjust to low concentrations, and therefore the measurement points 4 and 8% are excluded and 10% inserted. Pulses of hydrogen are applied to the gas sensor, see figure 5.3. Each concentration is applied for two minutes after which nitrogen is applied for two minutes. The sensor has time to stabilize and respond during these intervals.

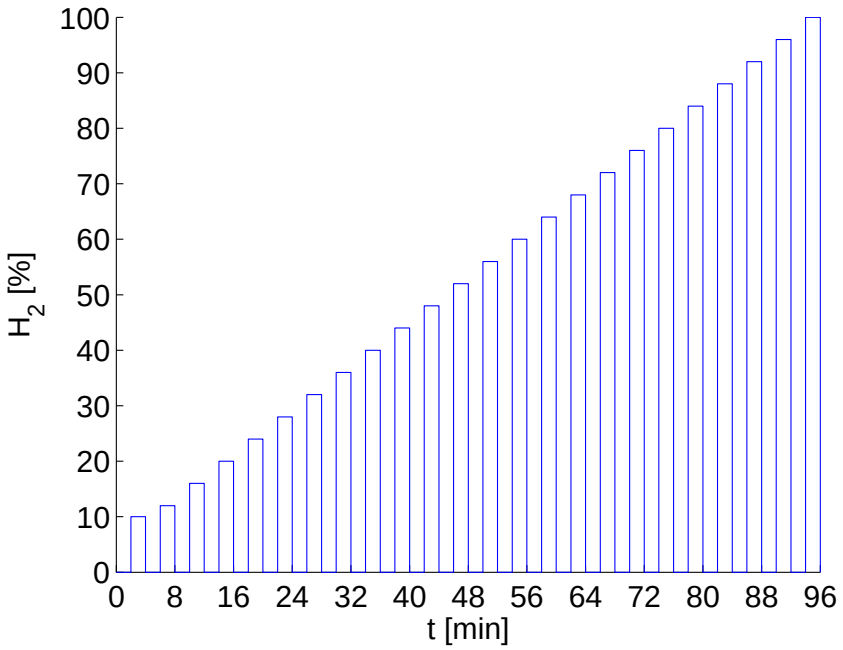

Figure 5.3: The hydrogen concentration versus time.

The temperature of the surrounding gas is varied between 30 and 120°C in steps of 10°C. The temperature 125°C is also applied to include the upper limit of the temperature range, specified in section 2.4. Each temperature is maintained for five hours, so that at least two series of hydrogen pulses will run when the system has stabilized on a new temperature. Figure 5.4 shows the temperature profile.

For each hydrogen concentration and temperature of the surrounding gas, the mean value of the power needed to maintain the chip temperature 140°C will

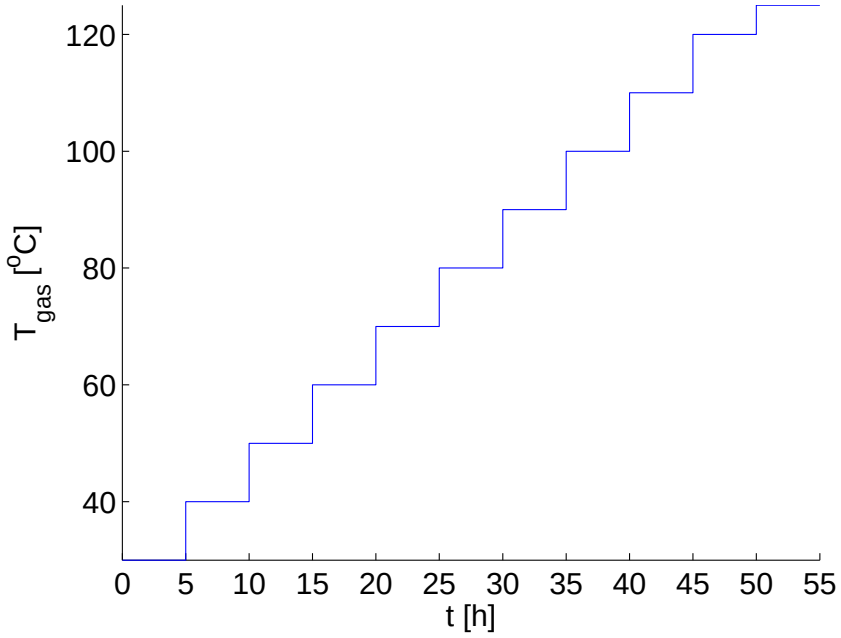

Figure 5.4: The temperature of the surrounding gas versus time.

be calculated from experimental parameters. Data will only be used when the sensor system has stabilized on a new hydrogen concentration and a new temperature.

5.3 Experimental Parameters

The parameters that are changed in the experiments are the concentration of hydrogen and the temperature of the surrounding gas. For each combination of these parameters, a mean value of the power input needs to be obtained. In this section, the parameters that determine the power input to the heaters are presented.

The temperature of the chip is kept constant by a PI-regulated feed-back coupling, governing the power input through a pulse width modulated heater circuit. The applied power alternates between P_{max} and 0, see figure 5.5. P_{max} varies somewhat between modules, and is therefore a source of errors. The value used is obtained from measurements. The frequency is constant, which means that the length of a period, called n_{tot}, is constant. n_{tot} is divided into 2^{16} discrete levels. n_{on} constitutes the part of n_{tot} where P_{max} is applied. The length of n_{on} varies between 0 and $0.9n_{tot}$, depending on how much power is needed, see figure 5.5. The frequency is much higher than the thermal time constant of the system, giving the heating an analog behaviour.

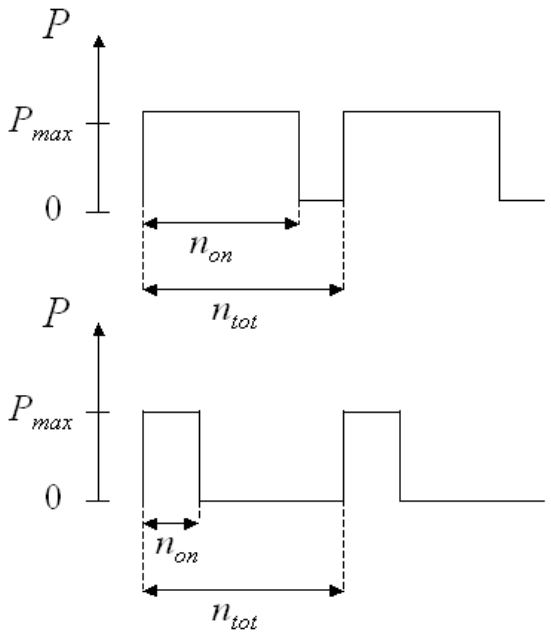

Figure 5.5: The applied power in the pulse width modulated heater circuit. The upper figure gives a high and the lower figure a low power input.

The effective power input is:

$$P_{effective} = P_{max}\frac{n_{on}}{n_{tot}} \ , \tag{5.1}$$

where

$$n_{on} = k_I I_{feed-back} + P_{feed-back} \tag{5.2}$$
$$n_{tot} = 2^{16} \ . \tag{5.3}$$

$P_{feed-back}$ and $I_{feed-back}$ are parameters in the PI-regulation, obtained from the data stored from the sensor module. k_I is a constant and its value depends on how the PI-regulation is tuned.

The mean value of the power input is obtained for different gas concentrations and different temperatures of the surrounding gas through the mean value of the effective power input.

5.4 Results

A graph of the mean value of the power input plotted against the concentration of hydrogen, for different values of the surrounding gas temperature, can be seen in figure 5.6. In figure 5.7, the mean value of the power input is plotted against the temperature of the surrounding gas, for different values of the hydrogen concentration.

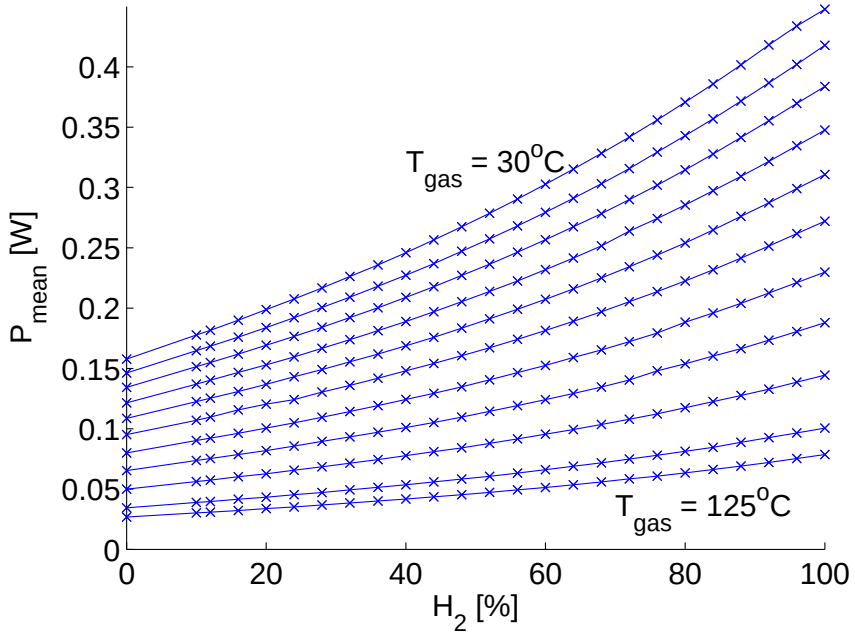

Figure 5.6: The mean value of the power input versus the hydrogen concentration for module A2012. Nitrogen is used as carrier gas. Each curve represents a certain temperature of the surrounding gas.

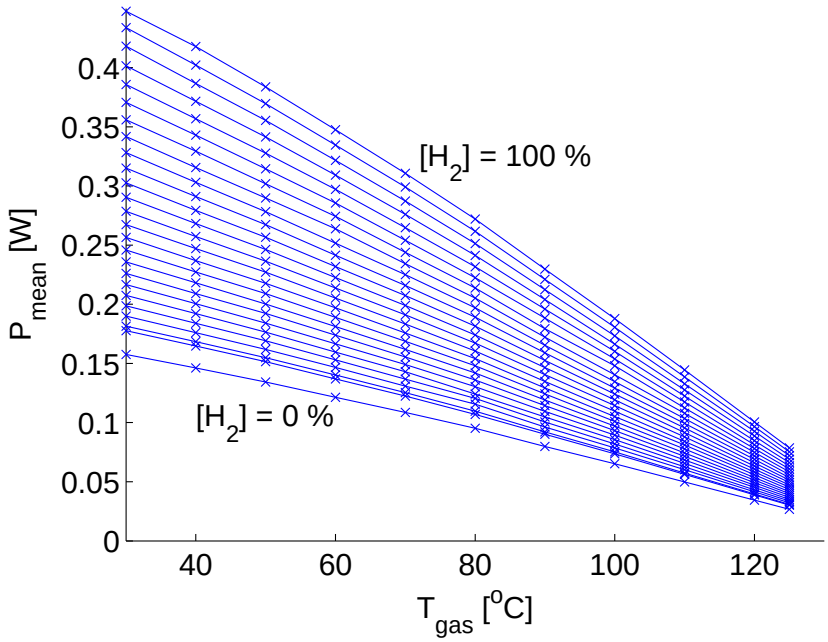

Figure 5.7: The mean value of the power input versus the temperature of the surrounding gas for module A2012. Each curve represents a certain concentration of hydrogen.

It is clear that the applied power increases with the increase in hydrogen concentration and the decrease in temperature. The hydrogen gas has a cooling effect. In heat transfer terms, it means that a large hydrogen concentration implies large convection from the surfaces of the sensor module. When the temperature of the gas decreases, more power is needed in order to maintain the constant chip temperature.

Chapter 6

Semi-Empirical Model

A great challenge in simulating heat transfer by convection is to find a model for the convection coefficient. Convection is a very complicated phenomenon, involving fluid flow over surfaces. In this chapter, the convection coefficient is obtained by a semi-empirical approach. Formulas for the convection coefficient found in the literature, obtained from systematic studies of the behaviour of convection on different surfaces, are used. The method is called semi-empirical in this report, as the formulas are developed from experiments, but with a theoretic understanding of convection. (A pure theoretic approach is very complicated and analytic expressions only exist for a few simple cases.) The result is presented and the model is compared to experimental data.

6.1 Semi-Empirical Convection Coefficient

There are many formulas for the convection coefficient in the literature that are obtained through experiments. The geometry, the temperatures of the gas and the surface, other properties of the gas and if the fluid flow is laminar or turbulent are parameters that influence the convection coefficient. An approach for finding the convection coefficient through using some of these empirical formulas is presented in this section.

There will be no wind or flow forced by external means in the gas sensor module, as the sensor house encloses all the surfaces and the gas can reach the chip only through a diffusion filter. In particular, the chimney prevents any turbulence within the sensor module to reach the chip and the glass carrier. The convection is therefore considered as natural. The computation of the convection coefficient is mainly based on the formulas for natural convection presented in [10]. The flow is regarded as laminar, which will be motivated later on in this section.

There are three dimensionless parameters; the Grashof number, the Prandtl number and the Nusselt number, that are used when calculating the convection coefficient. As natural convection is driven by the gravitational force, the convection coefficient is different for different orientations of the surfaces. There are three cases that need to be considered here: a horizontal surface facing upward, a horizontal surface facing downward and a vertical surface. The computation

of the Grashof and Prandtl numbers are identical for all geometries, while the computation of the Nusselt number differ.

The properties of the gas - the density ρ, the specific heat capacity at constant pressure c_p, the thermal conductivity k and the viscosity μ - are evaluated at the so called film temperature, T_{film}, which is the average of the surface and gas temperatures [10],

$$T_{film} = \frac{T_{surface} + T_{gas}}{2} \ . \tag{6.1}$$

The gas temperature is defined as the temperature of the gas at a long distance from the surface. How the gas properties are determined is described in section 2.3.

The Grashof number is [18]:

$$\mathrm{Gr} = \frac{g\beta\rho^2(T_{surface} - T_{gas})X^3}{\mu^2} \ , \tag{6.2}$$

where

$$\beta \approx \frac{1}{T_{film}} \tag{6.3}$$

for gases, g is the gravitational acceleration and X is the characteristic length of the system. For a horizontal surface, X is the area divided by the perimeter. For a vertical surface on the other hand, X is the length of the side in the vertical direction.

The Prandtl number is [18]:

$$\mathrm{Pr} = \frac{\mu c_p}{k} \ . \tag{6.4}$$

The Nusselt number can in the cases considered here be expressed by the formula [18]:

$$\mathrm{Nu} = C(\mathrm{GrPr})^n K + D \ , \tag{6.5}$$

where C, n, K and D depend on the geometry and on the value of GrPr. In table 6.1, the expressions for C, n, K and D for different geometries and different intervals of GrPr are specified. The values of GrPr for all surfaces in the sensor model lie in the range $10^{-1} < \mathrm{GrPr} < 10^3$. The formula for the horizontal plate facing downward in table 6.1, is not valid in this interval, but is used, as no other alternative is found in the literature.

The expression for the Nusselt number for the vertical plate is valid for laminar flow. The flow is considered laminar if $\mathrm{GrPr} < 10^9$ and turbulent if $\mathrm{GrPr} \geq 10^9$ [10]. As the values of GrPr lie in the range $10^{-1} < \mathrm{GrPr} < 10^3$, the flow is considered laminar for all surfaces.

The convection coefficient can now be expressed as [18]:

$$h = \frac{k\mathrm{Nu}}{X} \ . \tag{6.6}$$

The values of the convection coefficients for the upper horizontal surface and a vertical surface of the chip, see figure 6.1, will be computed for the chip temperature 140°C and the surrounding gas consisting of a mixture of hydrogen and nitrogen. The convection coefficients are plotted against the concentration of

Geometry	Gr Pr	C	n	K	D
Horizontal surface facing upward	$1 < \mathrm{GrPr} < 200$	0.96	$\frac{1}{6}$	1	0
Horizontal surface facing upward	$200 < \mathrm{GrPr} < 10^4$	0.59	$\frac{1}{4}$	1	0
Horizontal surface facing downward	$10^5 < \mathrm{GrPr} < 10^{10}$	0.27	$\frac{1}{4}$	1	0
Vertical surface	$\mathrm{GrPr} < 10^9$	0.67	$\frac{1}{4}$	$[1 + (\frac{0.492}{\mathrm{Pr}})^{\frac{9}{16}}]^{-\frac{4}{9}}$	0.68

Table 6.1: The Nusselt number for different geometries and different intervals of GrPr [10].

hydrogen gas, for different temperatures of the gas, in figures 6.2 and 6.3. In figures 6.4 and 6.5, the convection coefficients are plotted against the temperature for different hydrogen concentrations. The convection coefficients increase with increasing hydrogen concentration. This is expected, as it is known that hydrogen has a cooling effect. For the horizontal surface, the convection coefficient decreases with increasing temperature while the temperature has a very limited effect on the vertical surface.

In this context, it is important to emphasize the uncertainty in the computation of the convection coefficient. The empirical formulas are obtained from experiments on large and free surfaces, not surrounded by other objects. Most of the surfaces in the sensor model are very small and they are all enclosed by the sensor house. To use these formulas for the sensor module therefore implies a great uncertainty.

6.2 Results

The model is implemented and the equations are solved in FEMLAB with MATLAB, described in chapter 8. An understanding of the temperature distribution can be obtained from the solution. As an example, the temperatures of the surfaces, when the surrounding gas is nitrogen at 30°C, are presented in figures for different parts of the sensor model. In table 6.2, there is a list of the different temperatures and gas concentrations that need to be specified in the simulation.

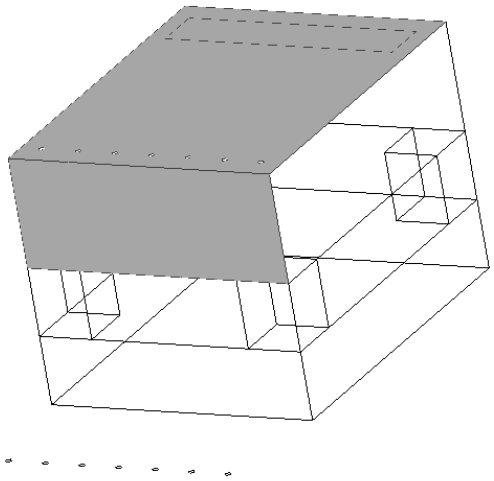

Figure 6.1: The convection coefficients for the gray surfaces are computed for different concentrations of hydrogen gas and different gas temperatures.

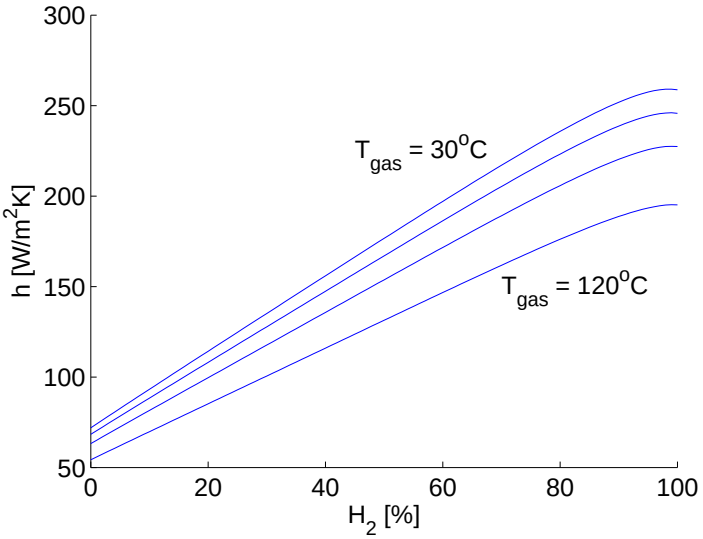

Figure 6.2: The convection coefficient plotted against the concentration of hydrogen gas for the upper horizontal surface of the chip. The temperature of the surrounding gas varies between 30 and 120°C in steps of 30°C.

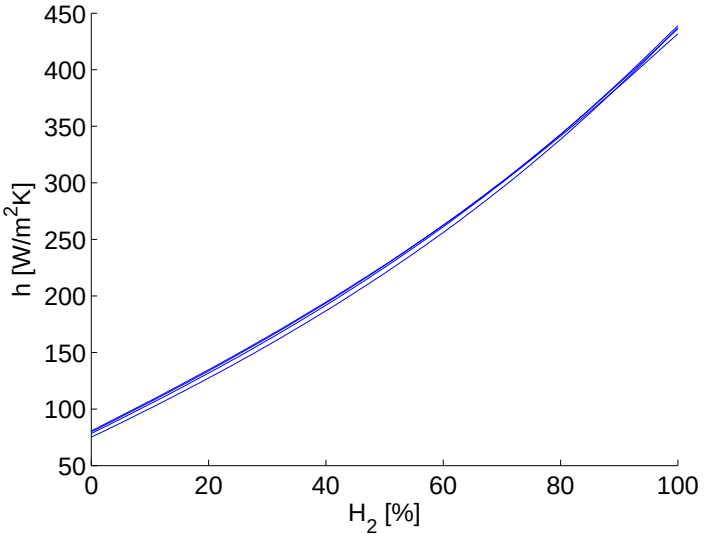

Figure 6.3: The convection coefficient plotted against the concentration of hydrogen gas for the vertical surface of the chip. The temperature of the surrounding gas varies between 30 and 120°C in steps of 30°C.

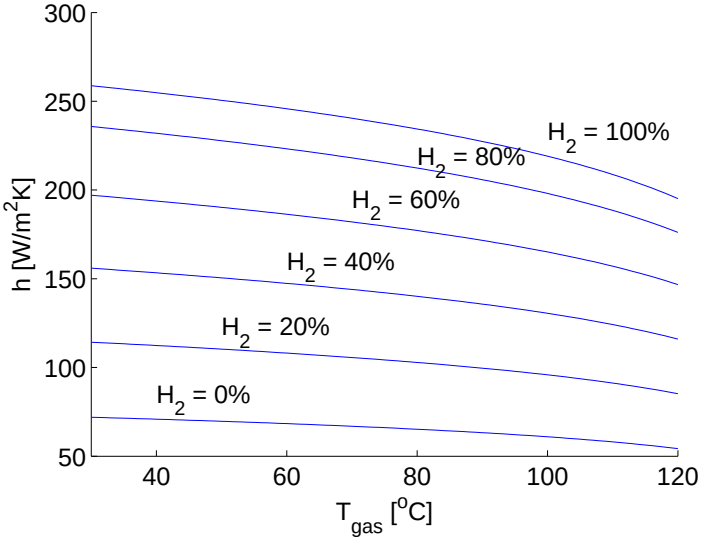

Figure 6.4: The convection coefficient plotted against the temperature of the surrounding gas for the upper horizontal surface of the chip. The hydrogen concentration varies between 0 and 100% in steps of 20%.

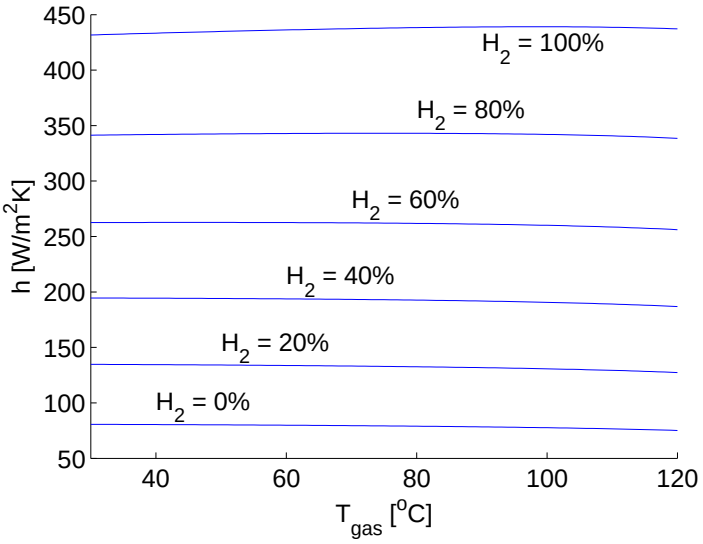

Figure 6.5: The convection coefficient plotted against the temperature of the surrounding gas for the vertical surface of the chip. The hydrogen concentration varies between 0 and 100% in steps of 20%.

The temperatures of the boundaries vary between 39 and 140°C, 39°C on the outer part of the PCB and 140°C on the heaters. A close-up of the chip and the glass carrier can be seen in figure 6.6. It is clear that the temperature gradient is largest on the glass carrier, which is expected as the glass carrier is used as an insulator. The temperature distribution on the upper surface of the chip is shown in figure 6.7. The temperature is rather homogeneous on the chip, with a gradient of only three degrees on the upper surface. On the points of attachment of the bond wires on the PCB, the temperature is much higher than on the rest of the PCB, which can be seen in figure 6.8.

The heat transfer from and to the chip, the glass carrier and the PCB can be obtained from the solution. It is decided to study the heat transfer for the chip temperature 140°C and the surrounding gas temperature 20°C, for 100% N_2 and 100% H_2, see table 6.3. The results are shown in tables 6.4 to 6.6. It is clear that the heat transfer due to radiation compared to convection from the chip and the glass carrier is very small, while it is significant from the PCB. When the hydrogen concentration is raised from 0 to 100%, the convection from the chip and the glass carrier is increased by several factors, while it is hardly not changed from the PCB.

The most important result is how the power input needed to maintain constant chip temperature varies with composition and temperature of the surrounding gas. A comparison between experiments and simulations will be made in the next section. The distribution between different modes of heat transfer from the chip in simulations compared to experiments will also be studied.

Parameter	Value
T_{gas}	30°C
$T_{ambient}$	T_{gas}
T_{chip}	140°C
N_2	100%
O_2	0%
H_2	0%

Table 6.2: Temperatures and gas composition when studying the surface temperatures of the sensor system.

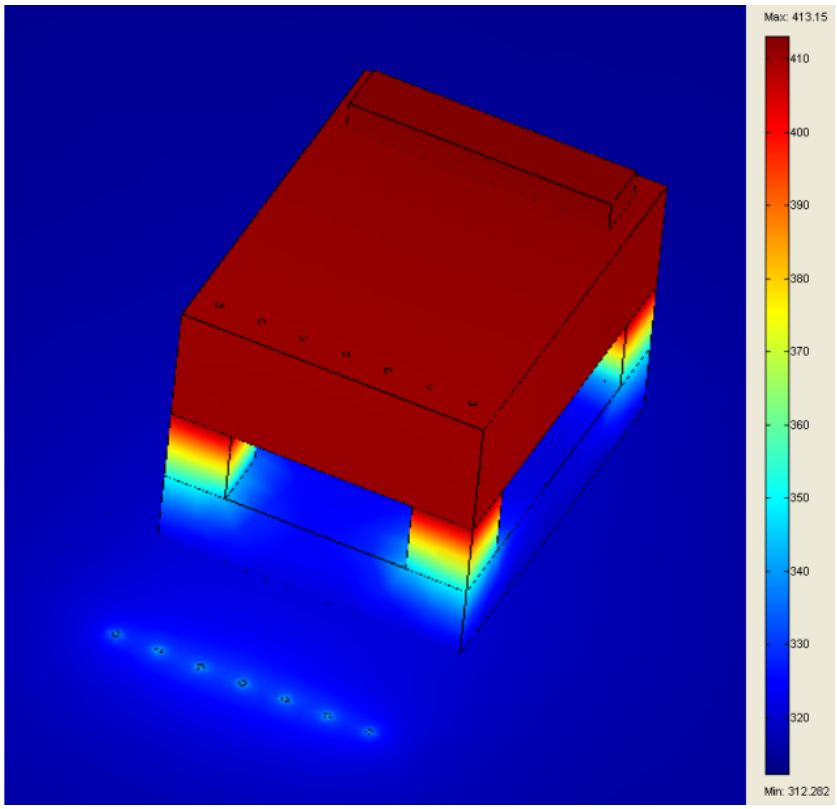

Figure 6.6: The temperature distribution on the chip and the glass carrier. The scale on the right shows which color corresponds to which temperature in Kelvin.

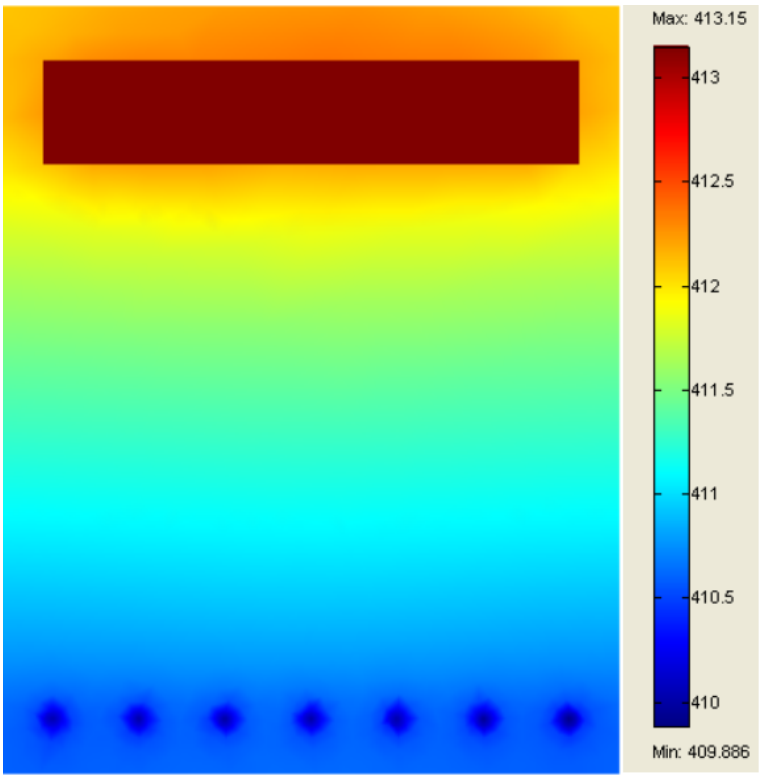

Figure 6.7: The temperature distribution on the upper surface of the chip.

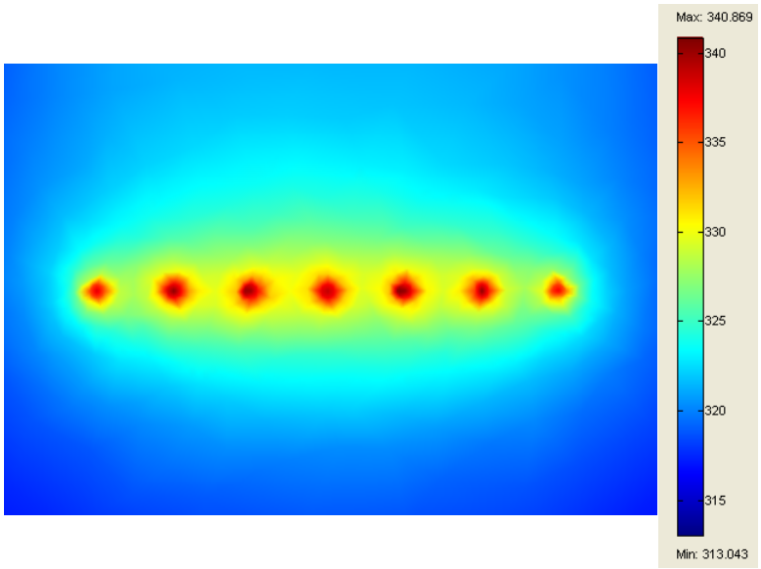

Figure 6.8: The temperature distribution on the points of attachment of the bond wires on the PCB.

Parameter	Value 100% N_2	Value 100% H_2
T_{gas}	20°C	20°C
$T_{ambient}$	T_{gas}	T_{gas}
T_{chip}	140°C	140°C
N_2	100%	0%
O_2	0%	0%
H_2	0%	100%

Table 6.3: Temperatures and gas compositions when studying the heat transfer from and to the different subdomains.

Heat transfer from and to chip	100% N_2 [mW]	100% H_2 [mW]
Convection	22	86
Radiation	3	3
Conduction to bond wires	55	57
Conduction to glass carrier	65	81
Power input	146	226

Table 6.4: Heat transfer from and to chip for 100% nitrogen and 100% hydrogen.

Heat transfer from and to glass carrier	100% N_2 [mW]	100% H_2 [mW]
Convection	7	33
Radiation	1	1
Conduction to PCB	57	47
Conduction from chip	65	81

Table 6.5: Heat transfer from and to glass carrier for 100% nitrogen and 100% hydrogen.

Heat transfer from and to PCB	100% N_2 [mW]	100% H_2 [mW]
Convection	66	69
Radiation	46	35
Conduction from bond wires	55	57
Conduction from glass carrier	57	47

Table 6.6: Heat transfer from and to PCB for 100% nitrogen and 100% hydrogen.

6.3 Semi-Empirical Model Compared to Experiments

6.3.1 Distribution between Modes of Heat Transfer on Chip

The first step is to compare the simulated distribution between heat transfer from the chip through convection, radiation, conduction to the bond wires and conduction to the glass carrier, with the experimental data presented in section 1.2. The experiment is carried out with the chip surrounded by air in room temperature. The simulation is performed with the same temperatures and gas concentrations as in the experiments, see table 6.7. The experimental and simulated values of heat transfer on the chip are shown in table 6.8.

Parameter	Value
T_{gas}	20°C
$T_{ambient}$	T_{gas}
T_{chip}	140°C
N_2	79%
O_2	21%
H_2	0%

Table 6.7: Temperatures and gas composition when studying the distribution between modes of heat transfer on the chip.

As the experiment is performed on an older version of the gas sensor module than the model is developed for, it is not the absolute values of the different modes of heat transfer or the total power input that are interesting. Instead, the

Heat transfer	Experiment [mW]	Experiment %	Simulation [mW]	Simulation %
Convection and radiation	42	32	(22 + 3)	(15 + 2)
Conduction to bond wires	28	22	55	38
Conduction to glass carrier	60	46	65	45
Power input	130	100	146	100

Table 6.8: Distribution between different modes of heat transfer on the chip in experiment and simulation.

distribution between the different modes is important to study. Heat dissipation through convection and radiation in the simulation constitutes 17% of the total power input. The corresponding figure is 32% in the experiment. The greatest uncertainty in the model is the computation of the convection coefficient. It is clear that the heat transfer through convection is too low in the simulation. The computation of the convection coefficient is therefore not satisfactory.

Furthermore, the heat transfer through conduction in the bond wires is too high in the simulation. Parameters that decide the amount of heat transfer through conduction in the bond wires are: the thermal conductivity, the cross section area and the length of the bond wires as well as the temperature difference between the points of attachment of the bond wires on the chip and the PCB, see equation (3.23). The uncertainty is greatest in the length of the bond wires and the temperature difference. It is difficult to measure the exact length, but the value given in section 2.1 is rather an overestimation than an underestimation. The heat transfer through conduction would become even larger if the value of the length was given a smaller value. Therefore, the uncertainty of the length does not explain the problem. The conclusion is that the temperature difference in the simulation is too large, giving large simulated amounts of heat transfer through the bond wires. It can be explained by the negligence of heating of other components on the PCB in the sensor model. A better value of the heat transfer by conduction through the bond wires would be obtained if these effects were included in the model, or compensated for by increasing the temperature of the PCB.

It is important to remember that the experiment was performed on a gold header instead of on a PCB, which makes the experimental distribution between different modes of heat transfer somewhat uncertain. Consequently, the deviation between experiments and simulations arises probably not only from the incomplete model.

6.3.2 Power Input for Different Hydrogen Concentrations and Temperatures of Surrounding Gas

The next step is to compare simulations with the experiments in chapter 5. Simulations are performed using the same conditions as in the experiments. Nitrogen and hydrogen are the components of the gas mixture. The hydrogen concentration is varied from 0 to 100% in steps of 10%, and the temperature of the surrounding gas from 30°C to 120°C in steps of 30°C. In table 6.9, the values of temperatures and gas compositions in the simulations are summarized.

Parameter	Value
T_{gas}	$[30 : 30 : 120]$°C
$T_{ambient}$	T_{gas}
T_{chip}	140°C
N_2	$[100 : -10 : 0]$%
O_2	0%
H_2	$[0 : 10 : 100]$%

Table 6.9: Temperatures and gas compositions when studying the power input for different hydrogen concentrations and temperatures of the surrounding gas.

In figure 6.9, the power input to the heaters is plotted against the hydrogen concentration for different temperatures of the surrounding gas. Both the experimental and simulated curves are shown.

The only mode of heat transfer directly affected by the increase in hydrogen concentration is the convection. An increased convection from the glass carrier and the PCB however, lowers the temperatures of these subdomains, causing the conduction from the chip to the glass carrier and the PCB to increase. The increased conduction from the chip corresponds to the increased convection from the glass carrier and the PCB. Consequently, the increased power input when the hydrogen concentration is raised, is due to the increased convection from all surfaces of the sensor model. The conclusion when studying figure 6.9 is that the convection, and therefore the convection coefficients, in the simulations are too small.

6.4 Using Expression for Vertical Convection Coefficient

The change in the convection coefficients for the upper horizontal and vertical surfaces of the chip, when the concentration of hydrogen is increased, are shown in figures 6.2 and 6.3. There are several factors that point towards the formula

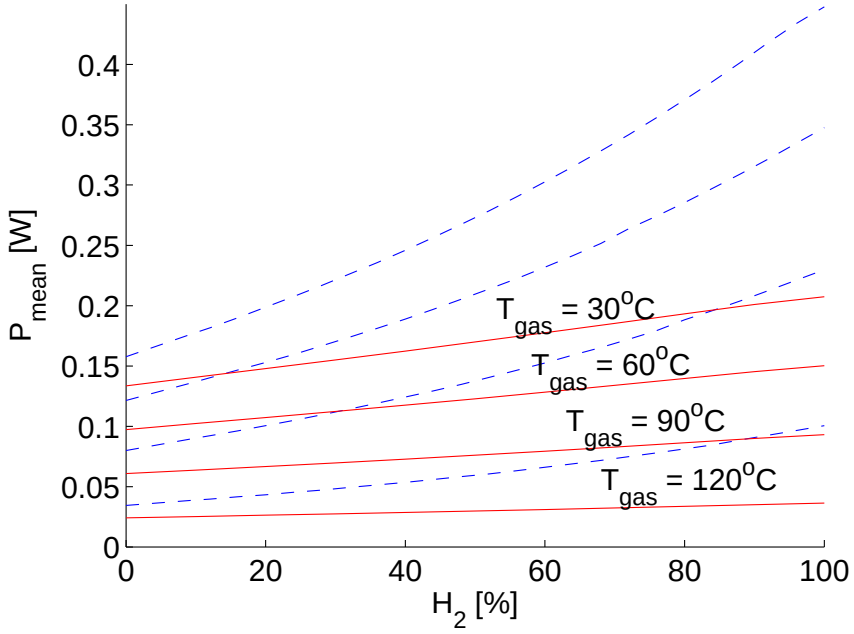

Figure 6.9: Power input plotted against hydrogen concentration for 30°C, 60°C, 90°C and 120°C. Experiments plotted with dashed lines and simulations with solid lines.

for the vertical convection coefficient being most suitable for describing the convection at all the surfaces of the chip and the glass carrier.

First of all, the vertical convection coefficient is larger than the horizontal, for all values of hydrogen concentration. It is clear that the computed convection coefficients in the previous sections are too small. Another factor is that the shape of the vertical convection coefficient in figure 6.3 is similar to the shape of the power plotted against the hydrogen concentration in the experiments, see figure 5.6.

Further on, only a small temperature dependence is observed for the vertical convection coefficient. This behaviour is expected when studying the experimental power consumption plotted against the temperature, for different concentrations of hydrogen, in figure 5.7. The curves are almost linear, implying that the convection coefficients only have a small temperature dependence, see Newton's law of cooling in equation (1.3).

Lastly, no orientation dependence has been observed experimentally. This indicates that the formulas for the convection coefficients should be rather similar for all orientations.

The computed convection coefficients on the small surfaces are more questionable than on the PCB, as the formulas used are obtained through experiments on surfaces of greater dimensions than the dimensions of the chip and the glass carrier. It is therefore worthwhile to use the formula for the vertical convection coefficient on all small surfaces, i.e. the surfaces of the chip and the glass carrier, and study the result. Simulations are performed for the same conditions as in section 6.3.2, and the resulting graph of the power plotted against the hydrogen concentration for different temperatures is shown in figure 6.10.

The simulated curves now have the correct shape, but the values of the power input are still too low. Even though this modification gives a better result than before, the simulations still do not completely correspond to the experiments.

6.5 Conclusion

It is not unexpected that the absolute values of heat transfer from the simulations do not match completely with the experiments. There are so many assumptions and simplifications made, that a certain deviation between experiments and simulations is expected. It would be more important to get a correct distribution between different modes of heat transfer and a correct behaviour of how the power input changes with the change in hydrogen concentration. A qualitative analysis is more important than a quantitative analysis, in order to understand the behaviour of the heat transfer on the gas sensor component and its closest surroundings.

Neither the qualitative nor the quantitative behaviour of the sensor model seem to match the experiments sufficiently. However, when using the expression for the vertical convection coefficient on the chip and the glass carrier, the sensor model matches the experiments qualitatively. Still, the change in convection when the hydrogen concentration is changed does not agree with experiments. The convection is too small, and the deviation from experiments increases with

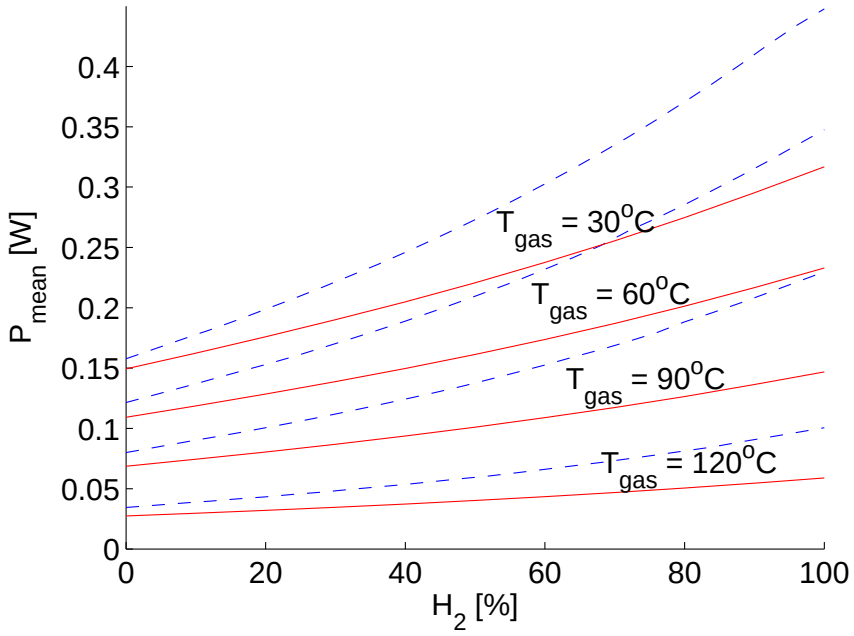

Figure 6.10: Power input plotted against hydrogen concentration for 30°C, 60°C, 90°C and 120°C. Experiments plotted with dashed lines and simulations with vertical convection coefficient on chip and glass carrier with solid lines.

increasing hydrogen concentration. The reason is that the computed convection coefficients are too small, especially for high hydrogen concentrations. Another problem is that the conduction through the bond wires is too large.

The conduction through the bond wires is described by well known physics. The model can be modified in order to simulate the conduction in a more satisfactory way, by including the heating effects of other components on the PCB. The most important question is therefore why the computed convection coefficients are incorrect. The convection coefficients do not increase sufficiently for increasing hydrogen concentrations. There might be several answers to this question and a few suggestions will be made here.

In the sensor module, the surfaces are surrounded by the sensor house and the convection takes place within enclosed volumes. The formulas for the convection coefficient assume that there are no objects close to the surfaces. The convection for free surfaces differ from the convection in bounded volumes. The heat transfer by natural convection in an enclosed volume is smaller however, than when there are no other other surfaces in the vicinity. Therefore, this is not the explanation of why the computed convection coefficients are too small. However, it might be necessary to include the fluid dynamics of the gas and describe the whole bounded system by equations to obtain a more accurate model.

The formulas for the convection coefficient found in the literature are empirical formulas developed for larger surfaces than the surfaces considered here. One might ask if they are still valid when the surface dimensions are very small-scale. The behaviour of hydrogen often differs from the behaviour of other gases, and the formulas might not be valid for high concentrations of hydrogen. It is also justified to question the validity of the formulas for the properties of gas mixtures when hydrogen is involved. The greatest remaining question is therefore if the problem lies in the small dimensions or in the non-ideal behaviour of hydrogen. It is probable however, that both these factors play an important role.

Chapter 7

Empirical Model

Since it turned out difficult to find the correct behaviour of the convection coefficient with the semi-empirical model, a new method is presented in this chapter. The convection coefficients are estimated from the experimental data, which is called the empirical approach. This model is restricted to the conditions for which the experiments are performed, which limits its usage. An important application area however, is simulation of heat transfer for time-dependent conditions. The empirical model is validated through comparison with experiments.

7.1 Empirical Convection Coefficient

The convection coefficients will be estimated from the experimental data. The experiments give a measure of how much the convection increases with the increase of hydrogen concentration and the change in temperature of the surrounding gas. This information can be used to estimate the convection coefficients. It is important to note that the empirical convection coefficient only includes convection, and not radiation. In the literature, a combined heat transfer coefficient including both convection and radiation is sometimes defined [6].

The model is developed for the inert mode, temperatures of the surrounding gas between 30 and 125°C, the chip temperature 140°C and the geometry and material properties specified in chapter 2. It will therefore be valid only for these conditions, which implies a restriction on the model.

Theoretically, the convection $\dot{Q}_{convection}$ from all surfaces $i = 1, ..., m$, can be expressed by:

$$\dot{Q}_{convection}(H,T) = \sum_i h_i(H,T) A_i (T_{surface,i} - T) \ , \tag{7.1}$$

where $\dot{Q}_{convection}$ varies with the hydrogen concentration H and the temperature T of the surrounding gas. $h_i(H,T)$ is the convection coefficient, A_i the area and $T_{surface,i}$ the temperature of surface i.

It would be too complicated to find the unique convection coefficients $h_i(H,T)$ for all surfaces. Therefore, it is assumed that the convection coefficients are

identical for all surfaces and temperatures of the surrounding gas, when there is no hydrogen present. In figure 5.7, the power consumption is plotted against the temperature for different concentrations of hydrogen. The curves are almost linear, which implies that the convection coefficients only have a small temperature dependence, see Newton's law of cooling in equation (1.3). The assumption that the convection coefficients are identical for all surfaces, and not dependent of the size or orientation of the surface in question, is an approximation that we have to keep in mind. h_0 denotes the convection coefficient for all surfaces when there is no hydrogen present. How h_0 is obtained is described in section 7.1.1. The expression for the convection can now be rewritten as:

$$\dot{Q}_{convection}(H,T) = \sum_i (h_0 + \Delta h_i(H,T)) A_i (T_{surface,i} - T) \ , \tag{7.2}$$

where $\Delta h_i(H,T)$ is the change in the convection coefficient for surface i when the hydrogen concentration is raised from 0 to $H\%$.

The change in convection when the hydrogen concentration is raised from 0 to $H\%$ is then:

$$\Delta\dot{Q}_{convection}(H,T) = \sum_i \Delta h_i(H,T) A_i (T_{surface,i} - T) \ . \tag{7.3}$$

The temperature of the chip is kept constant at T_{chip}. The temperatures on all other surfaces lie closer to the temperature of the surrounding gas. The change in convection for an increased hydrogen concentration is therefore largest on the chip, which is also clear from the simulation presented in tables 6.4 to 6.6. By assuming that only the convection coefficients on the surfaces of the chip are changed when the concentration of hydrogen is changed, and that the convection coefficient is identical for all surfaces of the chip, $\Delta h(H,T) \neq 0$ for the surfaces of the chip and $\Delta h = 0$ for all other surfaces. The change in convection can therefore be expressed as:

$$\Delta\dot{Q}_{convection}(H,T) = \Delta h(H,T) A_{chip} (T_{chip} - T) \ . \tag{7.4}$$

$\Delta\dot{Q}_{convection}(H,T)$ can be obtained from the experimental data, see section 7.1.2.

The change in the convection coefficient on the surfaces of the chip, when the hydrogen concentration is raised from 0% to $H\%$, is then:

$$\Delta h(H,T) = \frac{\Delta\dot{Q}_{convection}(H,T)}{A_{chip}(T_{chip} - T)} \ . \tag{7.5}$$

Empirical expressions for the convection coefficients can now be summarized as:

$$h(H,T) = h_0 + \frac{\Delta\dot{Q}_{convection}(H,T)}{A_{chip}(T_{chip} - T)} \ , \tag{7.6}$$

for the surfaces of the chip and

$$h(H,T) = h_0 \ , \tag{7.7}$$

for all other surfaces.

7.1.1 Finding h_0

As mentioned earlier, the convection coefficients are assumed to be identical for all surfaces and temperatures of the surrounding gas when there is no hydrogen present. Simulations are performed for different values of this convection coefficient h_0, and for different temperatures of the surrounding gas. In table 7.1, the temperatures and gas composition in the simulations are specified.

Parameter	Value
T_{gas}	[30 : 10 : 120], 125°C
$T_{ambient}$	T_{gas}
T_{chip}	140°C
N_2	100%
O_2	0%
H_2	0%

Table 7.1: Temperatures and gas composition when varying h_0.

The resulting power input is studied and compared to experimental data. h_0 is varied between 80 and 140W/m^{2}K in steps of 20W/m^{2}K, giving the result in figure 7.1. $h_0 = 100$W/m^{2}K seems to match experimental data well enough.

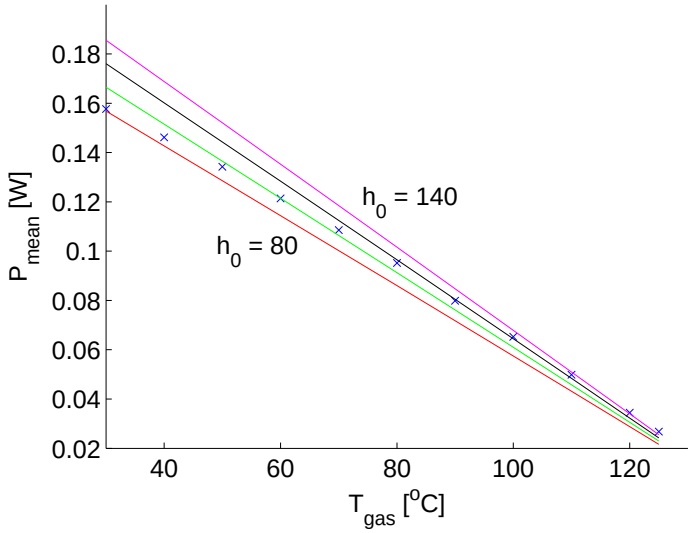

Figure 7.1: Power input plotted against temperature of surrounding gas. Experimental data plotted as x and empirical models with $h_0 = 80, 100, 120$ and 140W/m^{2}K with solid lines.

7.1.2 Finding $\Delta\dot{Q}_{convection}(H,T)$

Finally, the change in convection when the hydrogen concentration is raised from 0 to $H\%$, will be found from experimental data. As stated in section 6.3.2, the increased power input when the hydrogen concentration is raised, arises from the increased convection at all surfaces. The change in convection can therefore be expressed by:

$$\Delta\dot{Q}_{convection}(H,T) = \dot{Q}(H,T) - \dot{Q}(H=0,T)\ . \tag{7.8}$$

where $\dot{Q}(H,T)$ is the power input for $H\%$ hydrogen and the temperature T of the surrounding gas. An expression for how the power input varies with the hydrogen concentration and the temperature of the surrounding gas is searched. The curves in figure 5.6 and 5.7 show how the power input depends on the hydrogen concentration for a certain temperature, and on the temperature for a certain hydrogen concentration. It seems as if the curves can be approximately described by polynomials of second degree. There is also a certain dependence between the hydrogen concentration and the temperature. The following equation will therefore be fitted to the experimental data:

$$\dot{Q}(H,T) = x_1H^2 + x_2H + x_3T^2 + x_4T + x_5HT + x_6\ , \tag{7.9}$$

where x_1 to x_6 are unknown constants. The experimental data for $\dot{Q}(H,T)$ with the corresponding values of H and T are put into equation (7.9), giving:

$$\begin{pmatrix} \dot{Q}_{11} \\ \vdots \\ \dot{Q}_{n1} \\ \dot{Q}_{12} \\ \vdots \\ \dot{Q}_{n2} \\ \vdots \\ \dot{Q}_{1m} \\ \vdots \\ \dot{Q}_{nm} \end{pmatrix} = \begin{pmatrix} H_1^2 & H_1 & T_1^2 & T_1 & H_1T_1 & 1 \\ \vdots & \vdots & \vdots & \vdots & \vdots & \vdots \\ H_n^2 & H_n & T_1^2 & T_1 & H_nT_1 & 1 \\ H_1^2 & H_1 & T_2^2 & T_2 & H_1T_2 & 1 \\ \vdots & \vdots & \vdots & \vdots & \vdots & \vdots \\ H_n^2 & H_n & T_2^2 & T_2 & H_nT_2 & 1 \\ \vdots & \vdots & \vdots & \vdots & \vdots & \vdots \\ H_1^2 & H_1 & T_m^2 & T_m & H_1T_m & 1 \\ \vdots & \vdots & \vdots & \vdots & \vdots & \vdots \\ H_n^2 & H_n & T_m^2 & T_m & H_nT_m & 1 \end{pmatrix} \begin{pmatrix} x_1 \\ x_2 \\ x_3 \\ x_4 \\ x_5 \\ x_6 \end{pmatrix}\ . \tag{7.10}$$

This is an overdetermined system of equations with six unknowns. The least square method is used to find numerical values of x_1 to x_6.

In figure 7.2, the experimental data is plotted in the same graph as equation (7.9) with the values of x_1 to x_6 inserted. Equation (7.9) describes the behaviour of the power input, when the hydrogen concentration and the temperature are changed, sufficiently well.

The change in convection can be expressed by equation (7.11), obtained by inserting equation (7.9) into equation (7.8).

$$\Delta\dot{Q}_{convection}(H,T) = x_1H^2 + x_2H + x_5HT \tag{7.11}$$

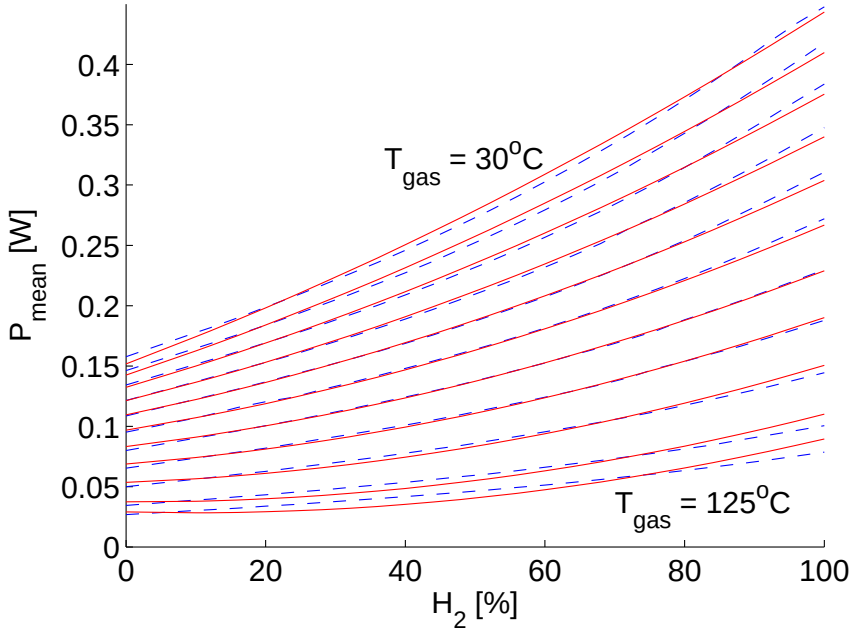

Figure 7.2: Power input plotted against hydrogen concentration for different temperatures. Experiments plotted with dashed lines and empirical model with solid lines.

7.2 Results

After implementing the model and solving the equations in FEMLAB with MATLAB, described in chapter 8, simulations can be performed. The temperature distribution has an appearance very similar to the temperature distribution in the semi-empirical model, see section 6.2.

The heat transfer from and to the chip, the glass carrier and the PCB for the same conditions as in section 6.2 are studied. (Note that the temperature of the surrounding gas is 20°C, which lies slightly below the temperature range for which the model has been developed.) The results are shown in tables 7.2 to 7.4. As the convection is assumed not to change on the glass carrier and the PCB when the hydrogen concentration is changed, it remains on the same level for 0 and 100% hydrogen. On the chip however, the convection is increased by a factor seven.

As for the semi-empirical model, the most important result is how the power input needed to maintain constant chip temperature varies with the composition and temperature of the surrounding gas. In the next section, comparisons between simulations and experiments will be made.

7.3 Empirical Model Compared to Experiments

7.3.1 Distribution between Modes of Heat Transfer on Chip

The distribution between different modes of heat transfer on the chip, presented in section 1.2, is compared to a simulation. The simulation is performed in the same way as for the semi-empirical model, described in section 6.3.1. In table 7.5, the results of the experiment and simulation are shown.

As noted in section 6.3.1, the absolute values are not interesting to study since the experiment is performed on another version of the gas sensor module than the model is developed for. The distribution between different modes of heat transfer in the simulation agrees quite well with the experiment. As for the semi-empirical model however, the conduction through the bond wires is too high, the reason being the same as described previously.

7.3.2 Power Input for Different Hydrogen Concentrations and Temperatures of Surrounding Gas

Simulations with the empirical convection coefficients are finally compared to the experiments presented in chapter 5. The simulations are performed in the same way as for the semi-empirical model, described in section 6.3.2. In figure 7.3, the power input to the heaters is plotted against the hydrogen concentration for different temperatures of the surrounding gas.

The experiments and the simulations do not agree completely, but well enough to confirm the validity of the empirical model. The model has not been validated by a new data set, which is common practice. This is not critical however, as

Heat transfer from and to chip	100% N_2 [mW]	100% H_2 [mW]
Convection	47	335
Radiation	3	3
Conduction to bond wires	60	58
Conduction to glass carrier	71	69
Power input	182	465

Table 7.2: Heat transfer from and to chip for 100% nitrogen and 100% hydrogen.

Heat transfer from and to glass carrier	100% N_2 [mW]	100% H_2 [mW]
Convection	10	9
Radiation	1	1
Conduction to PCB	61	59
Conduction from chip	71	69

Table 7.3: Heat transfer from and to glass carrier for 100% nitrogen and 100% hydrogen.

Heat transfer from and to PCB	100% N_2 [mW]	100% H_2 [mW]
Convection	116	112
Radiation	5	5
Conduction from bond wires	60	58
Conduction from glass carrier	61	59

Table 7.4: Heat transfer from and to PCB for 100% nitrogen and 100% hydrogen.

Heat transfer	Experiment [mW]	Experiment %	Simulation [mW]	Simulation %
Convection and radiation	42	32	(47 + 3)	(26 + 2)
Conduction to bond wires	28	22	60	33
Conduction to glass carrier	60	46	71	39
Power input	130	100	181	100

Table 7.5: Distribution between different modes of heat transfer on the chip in experiment and simulation with empirical convection coefficients.

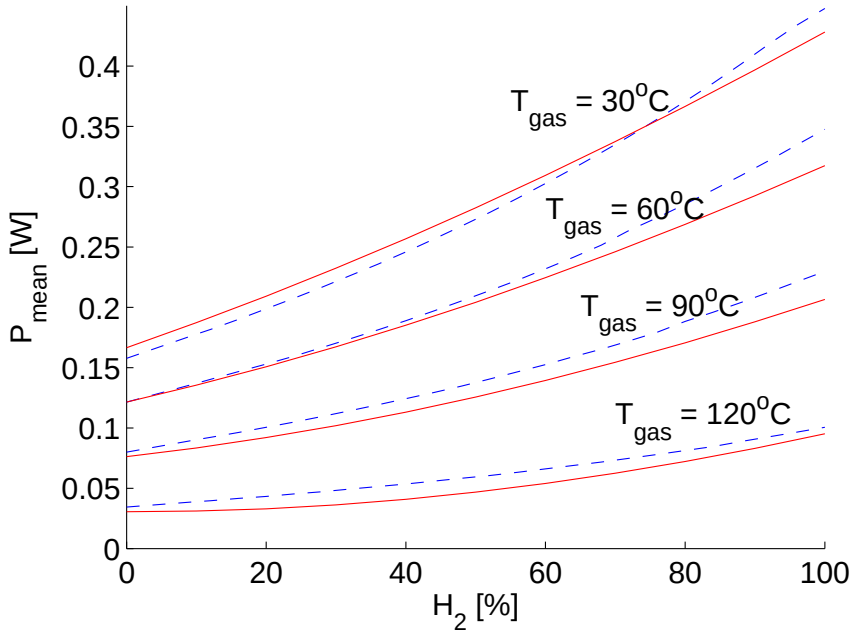

Figure 7.3: Power input plotted against hydrogen concentration for 30°C, 60°C, 90°C and 120°C. Experiments plotted with dashed lines and simulations with empirical convection coefficients with solid lines.

experience shows that the experimental data is practically repeatable and very stable.

7.4 Conclusion

The empirical model seems to agree well with experiments, except for the conduction through the bond wires, in spite of all the simplifications and assumptions made. The drawback of the model is the restriction to the conditions for which the experiments are performed. It is not possible to simulate other gas compositions than a mixture of nitrogen and hydrogen. Great care must be taken if the model is used to simulate changes in the dimensions or in the material properties and if it is used for temperatures of the surrounding gas below 30°C. However, the empirical model can be used reliably to simulate heat transfer on the gas sensor component for time-dependent conditions.

Chapter 8

Implementation in FEMLAB with MATLAB

In this chapter, the implementation of the models is described. It is mainly performed in FEMLAB, but an interface to MATLAB is used for certain calculations. The implementation of the semi-empirical and the empirical models are very similar, but parts specific for the semi-empirical model are indicated by *, while those specific for the empirical model are marked with **. This chapter goes into implementation details that can be left out when reading, without losing understanding for the rest of the report.

8.1 Modification of Sensor Model

Before the main steps in FEMLAB are described, the sensor model will be modified in order to obtain a solution of higher accuracy. The change concerns the modeling of the heaters.

As described so far, the heaters are represented by a two dimensional surface with a specified temperature boundary condition. The power input to the heaters corresponds to the normal heat flow into that surface. If this model would be implemented in FEMLAB, the computed normal heat flow into the surface would become inaccurate. The flux on the edges of the heaters would be divided between the surface representing the heaters and the surface representing the rest of the chip, even though the heat flow only originates from the heaters. Another problem is that the flux is not forced to be normal to the surface directly after passing through the surface, see figure 8.1. Both these problems give the computed normal heat flow an inferior value.

The sensor model is modified in order to obtain a greater accuracy of the power input to the heaters. The heaters are implemented as a subdomain instead of as a boundary. The new subdomain is placed on top of the chip and is made of the same material as the chip. The four vertical boundaries of the heaters are insulated and the upper surface is given the Dirichlet boundary condition of the chip temperature. This is a pure implementation technical modification,

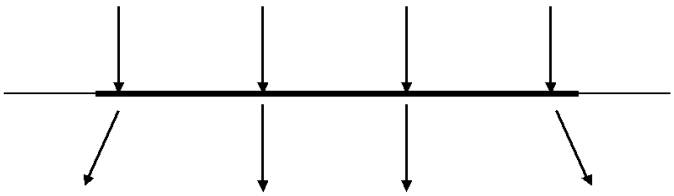

Figure 8.1: The heaters represented as a surface.

giving a more accurate value of the heat flow into the upper surface of the heaters, representing the power input, in the postprocessing in FEMLAB. The flow on the edges of the upper surface of the block, will belong only to the upper surface, as the adjacent surfaces are orthogonal to the heat flow. Another reason to why the flow computation becomes more accurate with this method, is that the flow into the upper surface and within the small subdomain will be forced to be normal to the horizontal surface, as the vertical surfaces are insulated, see figure 8.2. The computation of the normal heat flow will be much more accurate with this modified model.

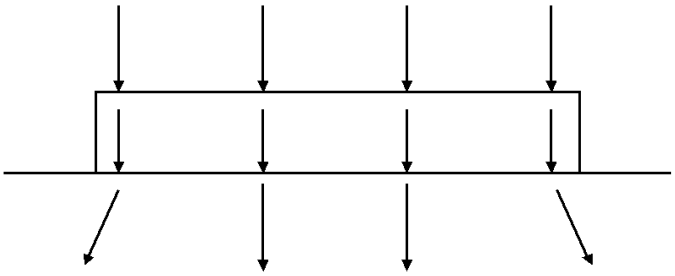

Figure 8.2: The heaters represented as a subdomain.

8.2 Main Modeling Steps in FEMLAB

In FEMLAB, there are six basic steps when creating a model and solving the equations [7]:

1. Creating or importing the geometry
2. Meshing the geometry
3. Defining the physics on the domains and at the boundaries
4. Solving the equations
5. Postprocessing the solution
6. Performing parametric studies

Details for all the steps in the semi-empirical and empirical models are described in sections 8.3 to 8.8. The default settings that are not changed are not accounted for.

8.3 Creating the Geometry

The first step is to create or import the geometry. The geometry of the sensor model is created directly in FEMLAB.

The chip is modeled as a solid block on which the heaters are represented as a smaller block. The upper surface of the heaters constitutes a boundary through which heat representing the power input can flow. The glass carrier is created as a composite object made out of four solid blocks, placed in the corners under the chip, and a solid block placed under the four blocks. The chip and the glass carrier are placed on a flat cylinder representing the PCB. The upper surface of the cylinder consists of two boundaries; an inner circle representing the part of the PCB inside the chimney and an outer segment representing the part of the PCB outside the chimney. The points of attachment of the bond wires on the chip and on the PCB are created as circular boundaries through which a heat flow can be defined. The dimensions of the chip, the glass carrier, the PCB and the boundaries representing the bond wires are described in section 2.1. The dimensions of the heaters in the xy-direction are specified in the same section and the size of the heaters in the z-direction is given the value $100 \cdot 10^{-6}$ m, large enough not to cause an ill-conditioned problem. In figure 8.3 the whole geometry is depicted and in figure 8.4 a close-up of the chip and the glass carrier with the corresponding boundaries can be seen.

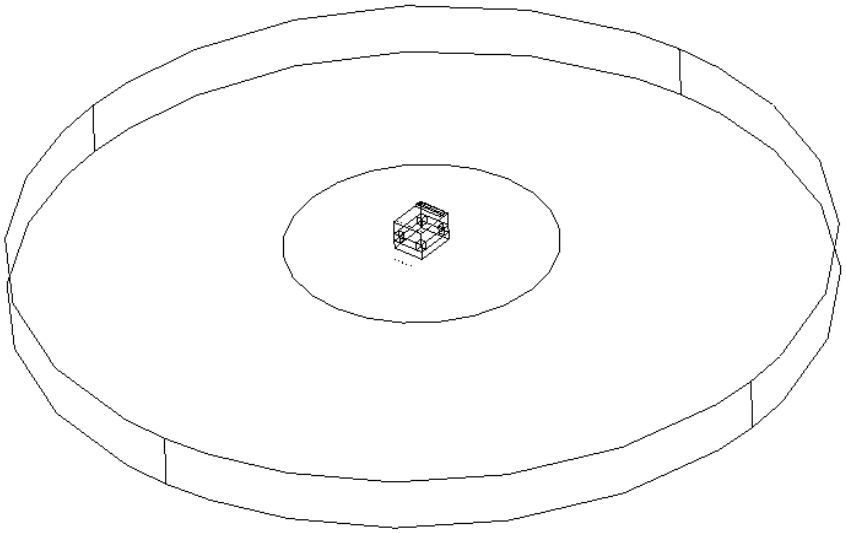

Figure 8.3: The geometry.

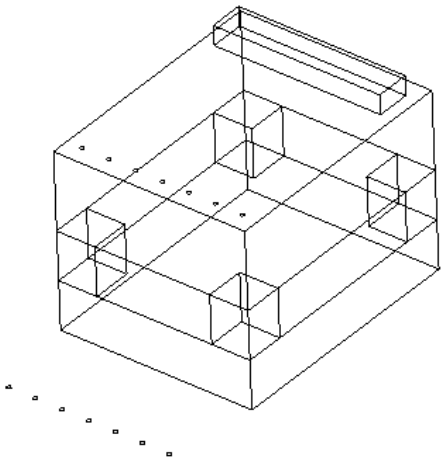

Figure 8.4: A close-up of the geometry of the chip and the glass carrier.

The model consists of the four subdomains described above; the chip, the heaters, the glass carrier and the PCB. Each subdomain is created in "the conduction application mode" in FEMLAB. This mode models heat transfer by conduction in the actual subdomains and takes into account heat transfer by convection and radiation at the boundaries. The bond wires are represented as boundaries and their influence is described by the boundary conditions.

8.4 Meshing the Geometry

The meshing of the geometry is performed using the default settings, except at the points of attachment of the bond wires, where the mesh is made finer in order to make the calculations more exact. The maximum element size is put to $2 \cdot 10^{-5}$ in `Mesh` $\rightarrow$ `Mesh Parameters` $\rightarrow$ `Boundary` for the boundaries representing the points of attachment of the bond wires. In figure 8.5, a close-up of the mesh at the chip, the glass carrier and the part of the PCB closest to the glass carrier is depicted.

The number of degrees of freedom can be found in `Mesh` $\rightarrow$ `Mesh Statistics`. For the sensor model, the number is approximately 4700, which is the number of unknowns in equation $\boldsymbol{K}\boldsymbol{a} = \boldsymbol{f}$, see section 4.7.

8.5 Defining the Physics

The physics in the subdomains and on the boundaries are defined in this section. In the subdomains, the physics is described by the heat equation, and on the boundaries by the boundary conditions. Certain constants, expressions and variables are specified before the settings in the subdomains and on the boundaries are made.

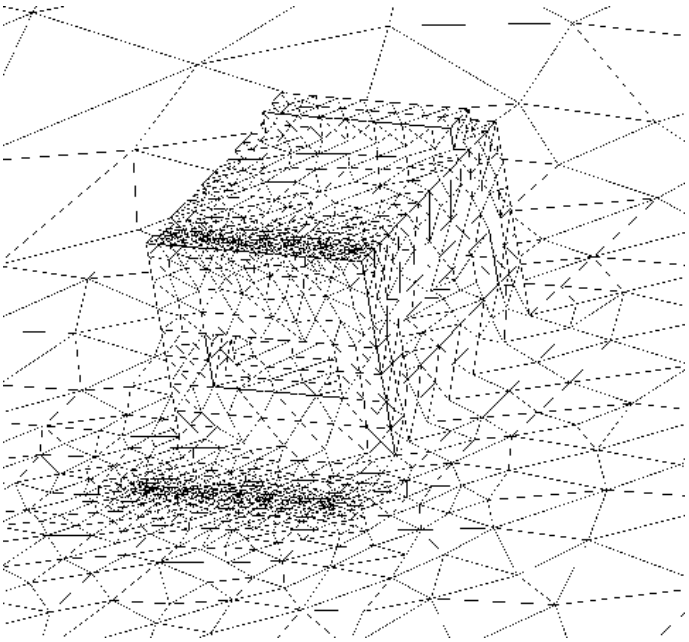

Figure 8.5: The mesh.

8.5.1 Constants

A list of constants is defined in `Options` → `Constants`. In table 8.1, constants defining geometrical sizes are listed and the numerical values are given in section 2.1. Most of these dimensions are needed when computing the convection coefficients in the semi-empirical model. Constants representing material properties are listed in table 8.2. These values can be found in section 2.2 except for the Stefan-Boltzmann constant that has the value $5.6705 \cdot 10^{-8}$ W/m^{2}K^4 [13]. The convection coefficient h_0 for the empirical model is also given in this table, and the value can be found in section 7.1.1. The temperatures of the heaters, the surrounding gas and the inside surface of the gas sensor module as well as the gas composition are defined in table 8.3. These constants are varied between simulations.

8.5.2 Scalar Expression

A scalar expression, `delta_h_conv`**, is defined in `Options` → `Expressions` → `Scalar Expressions`. It represents the change in the convection coefficient on the chip, $\Delta h(H, T)$, in the empirical model. It is computed by the MATLAB function `compute_deltah_empirical`**, see section 8.9.3.

8.5.3 Boundary Expressions

Boundary expressions are specified in `Options` → `Expressions` → `Boundary Expressions`. The value of a boundary expression is defined separately for each

Name	Description
chip_X*	size of chip in x-direction [m]
chip_Y*	size of chip in y-direction [m]
chip_Z*	size of chip in z-direction [m]
heaters_X*	size of heaters in x-direction [m]
heaters_Y*	size of heaters in y-direction [m]
glass_large_X*	size of glass carrier in x-direction [m]
glass_large_Y*	size of glass carrier in y-direction [m]
glass_large_Z*	size of lower part of glass carrier in z-direction [m]
glass_small_X*	size of column of glass carrier in x-direction [m]
glass_small_Y*	size of column of glass carrier in y-direction [m]
glass_small_Z*	size of column of glass carrier in z-direction [m]
PCB_real_X*	size of real PCB in x-direction [m]
PCB_real_Y*	size of real PCB in y-direction [m]
PCB_model_radius*	radius of modeled PCB [m]
gas_radius*	radius of chimney [m]
number_bond_wires*	number of bond wires
bond_wire_radius*	radius of bond wire [m]
bond_wire_length	length of bond wire [m]
bond_wire_constant	k_gold divided by bond_wire_length $[\frac{\mathrm{W}}{\mathrm{m}^2\mathrm{K}}]$

Table 8.1: Geometric constants.

Name	Description
`k_gold`	conductivity of gold $[\frac{\mathrm{W}}{\mathrm{mK}}]$
`s_b_constant`	Stefan-Boltzmann constant $[\frac{\mathrm{W}}{\mathrm{m^2K^4}}]$
`emissivity_SiO2`	emissivity of SiO_2
`emissivity_pyrex`	emissivity of pyrex
`emissivity_lacquer`	emissivity of lacquer
`h0_conv`**	convection coefficient h_0 for empirical model

Table 8.2: Material constants.

Name	Description
`Tinf`	temperature of surrounding gas, T_{gas} [K]
`Tamb`	temperature of inside surface of gas sensor module, $T_{ambient}$ [K]
`Theaters`	temperature of heaters (approximate temperature of chip), T_{chip} [K]
`N2`	volume fraction of nitrogen [%]
`O2`	volume fraction of oxygen [%]
`H2`	volume fraction of hydrogen [%]

Table 8.3: Constants defining temperatures and gas composition.

boundary.

There are three boundary expressions in the semi-empirical sensor model; `boundary_area*`, `X*` and `h_conv*`. `boundary_area*` defines the area and `X*` the characteristic length of the actual boundary with the help of the geometric constants defined in table 8.1. These boundary expressions are used in the computation of the convection coefficients. `h_conv*` defines the convection coefficient for the boundary in question by a call to the MATLAB function `compute_h*`, see section 8.9.1.

8.5.4 Boundary Integration Variables

In `Options` → `Integration Coupling Variables` → `Boundary Variables`, integration variables for boundaries are defined. An integration variable for a boundary designates the integral of a chosen expression over the boundary in question.

`Tmeanp*` is the mean temperature of boundary number p, which is computed as the integral of the temperature divided by the boundary area. It is defined for all boundaries exposed to the surrounding gas except for the heaters, i.e. all surfaces from which convection takes place. It is used in the computation of the semi-empirical convection coefficient.

`Power` is the power input on the upper boundary representing the heaters, which is computed as the integral of the normal heat flow into that surface. To get an accurate value, the normal heat flow is obtained through integration of the lagrange multiplier `lm1`, see section 8.5.8.

8.5.5 Boundary Extrusion Variables

Extrusion variables for boundaries map values from one boundary to another. They are defined in `Options` → `Extrusion Coupling Variables` → `Boundary Variables`.

`Tp` is the temperature on the bond wire attachment on the chip designated boundary number p, that can be reached from the corresponding bond wire attachment on the PCB and vice versa. This is necessary in order to define the boundary conditions on the points of attachment of the bond wires.

8.5.6 Subdomain Settings

The physics in the four subdomains is defined by the heat equation (3.3) containing the thermal conductivity. The heat equation for time-dependent conditions (3.1), also includes the density and the specific heat capacity. In order to facilitate an extension of the model to time-dependent conditions, all three material properties are defined in the FEMLAB model.

In `Options` → `Material Library` there is a predefined library for certain material properties. A new library is created where the thermal conductivity, the density and the specific heat capacity for silicon, pyrex and the PCB, presented

in section 2.2, are defined. The properties for each subdomain are loaded from the library material to `Physics` → `Subdomain Settings` → `Physics`.

The initial values of the temperatures in the subdomains are set in `Physics` → `Subdomain Settings` → `Init`. The initial temperature on the chip and the heaters is given the value of T_{chip}. On the glass carrier and the PCB, the initial temperature is put to 20°C. These values are used as the starting guess for the temperatures in the parametric solver, see section 8.8.

In `Physics` → `Subdomain Settings` → `Element`, the predefined elements are chosen as `Lagrange - Linear` for each subdomain, i.e. the approximating function is a linear polynomial.

8.5.7 Boundary Settings

The boundary conditions are defined in section 3.4. In FEMLAB, there are four types of boundary conditions to choose among; `heat flow` (corresponds to equation (3.16)), `thermal insulation` (corresponds to equation (3.10)), `temperature` (corresponds to equation (3.8)) and `zero temperature` (corresponds to equation (3.8) with $T_0 = 0$). All but `zero temperature` are used in the sensor model.

In `Physics` → `Boundary Settings`, the boundary conditions are set according to the list below, where the boundary conditions from section 3.4 are repeated with the defined names of constants, expressions and variables.

1. Envelope surface of PCB and vertical surfaces of heaters (FEMLAB: `thermal insulation`):
$$\boldsymbol{n} \cdot (\boldsymbol{k} \nabla T) = 0 \tag{8.1}$$

2. Upper surface of heaters (FEMLAB: `temperature`):
$$T = \texttt{Theaters} \tag{8.2}$$

3. Points of attachment of bond wires on chip where `Tp` is the temperature of corresponding point of attachment on PCB (FEMLAB: `heat flow`):
$$\boldsymbol{n} \cdot (\boldsymbol{k} \nabla T) = \texttt{bond\_wire\_constant}(\texttt{Tp} - T) \tag{8.3}$$

4. Points of attachment of bond wires on PCB where `Tp` is the temperature of corresponding point of attachment on chip (FEMLAB: `heat flow`):
$$\boldsymbol{n} \cdot (\boldsymbol{k} \nabla T) = \texttt{bond\_wire\_constant}(\texttt{Tp} - T) \tag{8.4}$$

5. All other surfaces of chip (FEMLAB: `heat flow`):
$$\begin{aligned} \boldsymbol{n} \cdot (\boldsymbol{k} \nabla T) &= \texttt{h\_conv}^*(\texttt{Tinf} - T) \\ &+ \texttt{emissivity\_SiO2} \cdot \texttt{s\_b\_constant}(\texttt{Tamb}^4 - T) \end{aligned} \tag{8.5}$$
$$\begin{aligned} \boldsymbol{n} \cdot (\boldsymbol{k} \nabla T) &= (\texttt{h0\_conv}^{**} + \texttt{delta\_h\_conv}^{**})(\texttt{Tinf} - T) \\ &+ \texttt{emissivity\_SiO2} \cdot \texttt{s\_b\_constant}(\texttt{Tamb}^4 - T) \end{aligned} \tag{8.6}$$

6. All other surfaces of glass carrier (FEMLAB: `heat flow`):

$$\begin{aligned} \boldsymbol{n}\cdot(\boldsymbol{k}\nabla T) &= \texttt{h\_conv}^{*}(\texttt{Tinf}-T) \qquad (8.7)\\ &+ \texttt{emissivity\_pyrex}\cdot\texttt{s\_b\_constant}(\texttt{Tamb}^4-T)\\ \boldsymbol{n}\cdot(\boldsymbol{k}\nabla T) &= \texttt{h0\_conv}^{**}(\texttt{Tinf}-T) \qquad (8.8)\\ &+ \texttt{emissivity\_pyrex}\cdot\texttt{s\_b\_constant}(\texttt{Tamb}^4-T) \end{aligned}$$

7. All other surfaces of PCB (FEMLAB: `heat flow`):

$$\begin{aligned} \boldsymbol{n}\cdot(\boldsymbol{k}\nabla T) &= \texttt{h\_conv}^{*}(\texttt{Tinf}-T) \qquad (8.9)\\ &+ \texttt{emissivity\_lacquer}\cdot\texttt{s\_b\_constant}(\texttt{Tamb}^4-T)\\ \boldsymbol{n}\cdot(\boldsymbol{k}\nabla T) &= \texttt{h0\_conv}^{**}(\texttt{Tinf}-T) \qquad (8.10)\\ &+ \texttt{emissivity\_lacquer}\cdot\texttt{s\_b\_constant}(\texttt{Tamb}^4-T) \end{aligned}$$

8.5.8 Weak Constraints

"The weak constraints feature in FEMLAB implements constraints by using finite elements on the constraint domain for the Lagrange multipliers, and by solving for the Lagrange multipliers along with the original problem." [7, User's Guide, Analysis Guide, Using Weak Constraints]. Weak constraints are used to obtain more accurate flux calculations on the upper surface of the heaters. They can only be used on boundaries specified by Dirichlet boundary condition. In `Physics` → `Properties` the `Weak constraints: Ideal` are chosen. The variable to be integrated when computing the normal heat flow in the post-processing is the lagrange multiplier called `lm1`.

8.6 Solving the Equations

The solver `Stationary nonlinear` is chosen in `Solve` → `Solver Parameters` → `General` → `Solver`. This solver is used as the problem is solved for steady-state conditions and the boundary conditions including radiation are non-linear. The algorithm is based on a damped Newton method. A Newton step is computed using the linear solver described below. Only the fraction of the Newton step determined by the damping factor is taken [7]. When parametric studies are performed (see section 8.8), the solver `Parametric nonlinear` is chosen instead.

Even if the problem is non-linear, most of the computer capacity is spent on solving systems of linear equations. A linear system solver needs to be specified in `Solve` → `Solver Parameters` → `General` → `Linear system solver`. There are direct and iterative methods to choose among. The direct solvers are appropriate for smaller problems and the iterative solvers for larger problems where the direct solvers need to much memory. The iterative methods do not always converge. Large three dimensional problems are often too memory consuming for direct solvers, but this problem is small enough to solve with a direct method. `Direct(UMFPACK)` is chosen, which is a "highly efficient direct solver for unsymmetric systems". "It solves general systems of the form Ax = b

using the unsymmetric-pattern multifrontal method and direct LU factorization of the sparse matrix A. It employs the COLAMD and AMD approximate minimum degree preordering algorithms to permute the columns so that the fill-in is minimized. The code, written in C, uses level-3 BLAS (Basic Linear Algebra Subprograms) for optimal performance." [7, User's Guide, Solving the Model, The Linear System Solvers].

Next, a solution form needs to be specified in `Solve` → `Solver Parameters` → `General` → `Solution form`. It "determines the form into which FEMLAB converts a PDE and its boundary conditions before solving it" [7, User's Guide, Solving the Model, Solver Overview]. The solution form `Weak`, which is the fastest and the most general solution form, is chosen.

The initial value is chosen as `Current solution` in `Solve` → `Solver Manager` → `Initial Value`, meaning that the current solution is used as a start guess the next time the model is solved.

8.7 Postprocessing the Solution

Postprocessing involves studying different plots and numerical values obtained from the solution. To obtain a surface plot showing the surface temperatures of the subdomains, `Postprocessing` → `Quick Plots` → `Boundary Plot` is chosen. Many other types of plots are available.

It is important to study the numerical values of the normal heat flow from or to the different boundaries caused by conduction in the bond wires, convection or radiation. This is possible through integrating a boundary condition, or part of a boundary condition, over one or several boundaries in `Postprocessing` → `Boundary Integration`. To study the power input to the heaters, the lagrange multiplier `lm1` is integrated over the upper surface of the heaters.

8.8 Performing Parametric Studies

When performing parametric studies, the equations corresponding to a sequence of FEMLAB models arising when one parameter is varied are solved. The parameters of interest in the sensor model are the hydrogen concentration and the temperature of the surrounding gas. In `Solve` → `Solver Parameters` → `General` → `Solver` the solver `Parametric nonlinear` is chosen. In `Solve` → `Solver Parameters` → `General` → `Parameter`, the name of the parameter `H2` or `Tinf` and a list of parameter values are specified.

8.9 Implementation in MATLAB

The computation of the convection coefficients in the semi-empirical and empirical models are performed in MATLAB.

8.9.1 Computation of Convection Coefficient in Semi-Empirical Model

The computation of the convection coefficient `h_conv*`, described in section 6.1, is carried out in the MATLAB function `compute_h*`. The in parameters are: the characteristic length of the surface (`X*`), the mean temperature of the surface (`Tmeanp*`), the temperature of the surrounding gas (`Tinf`), the direction of the surface and the concentrations of nitrogen (`N2`), oxygen (`O2`) and hydrogen (`H2`) in percentage by volume. The function calls the MATLAB function `properties*` that computes the properties of the gas at the film temperature.

8.9.2 Computation of Gas Properties in Semi-Empirical Model

The MATLAB function `properties*` computes the viscosity, the thermal conductivity, the specific heat capacity and the density of a gas mixture consisting of nitrogen, oxygen and hydrogen at a specified temperature, see section 2.3.1. The in parameters are the concentrations of the gas components in volume fraction and the temperature at which the computation is to be carried out.

8.9.3 Computation of Change in Convection Coefficient in Empirical Model

Through a call to the MATLAB function `compute_deltah_empirical**` with the in parameters the temperature of the surrounding gas (`Tinf`) and the concentration of hydrogen (`H2`), the change in the convection coefficient `delta_h_conv**` is computed. How the computation is performed is described in section 7.1.

Chapter 9

Conclusion and Future Work

The aim of the diploma work has been to simulate the different modes of heat transfer in the sensor system. Heat is transferred by conduction within and between the chip, the glass carrier and the PCB as well as by convection and radiation from all the surfaces. In this final chapter, conclusions and future work are discussed.

9.1 Conclusion

The greatest challenge in the diploma work has been to obtain a model for the convection coefficient. First, a semi-empirical approach was attempted. When comparing the model with experiments, it turned out that this method did not describe the behaviour of the convection well enough. Formulas for the convection coefficient found in the literature are apparently not fully applicable to the sensor system, the reason probably being the small dimensions of the chip and the glass carrier as well as the non ideal behaviour of hydrogen.

Next, the convection coefficient was found by an empirical approach. The simulations and experiments agreed well with this method. However, there are many assumptions and simplifications in the empirical model that one should keep in mind when using this model.

The heat transfer through conduction in the bond wires is too high in both the created models. The reason is a too large temperature difference between the points of attachment of the bond wires. The simulated temperatures of the PCB are too low and do not give a complete description of reality.

A justified question is whether the assumptions and simplifications are too large. Some of the simplifications that are made, might have to be modified in order to obtain a more reliable model. The heating of the PCB by other components has just been mentioned. Another example lies in neglecting the heating of the gas in the vicinity of the gas sensor model. The temperature of the gas close to the PCB is approximated to be equal to the temperature far away from the sensor. In reality, the gas is probably heated considerably, and this effect

could be included in the model. The restriction of the model to the chip, the glass carrier, the bond wires and the PCB can be questioned. Maybe the fluid dynamics of the gas should be included and the whole enclosed system described by equations.

However, there are many interesting conclusions that can be drawn from the performed simulations. One example is that the temperature distribution on the chip is rather homogeneous. The temperature gradient is only a few degrees. Another observation is that the heat transfer due to radiation on the chip and the glass carrier is insignificant, but of importance on the PCB. When considering the heat transfer from the chip, the radiative part can therefore be neglected.

The aim of the diploma work was to simulate the different modes of heat transfer in the sensor system. The goal is not entirely fulfilled as it turned out to be more difficult than expected to find a model for the convection. However, two models have been created and they both give interesting information. A comprehension of the distribution between conduction, convection and radiation has been obtained through this work.

9.2 Future Work

In order to continue the project at the company, it is important to get a better understanding of the convection coefficient. It is clear that the formulas used in this diploma work do not give a satisfactory description of the behaviour of the coefficient. It seems to be necessary to study the fluid dynamics of the gas inside the sensor module.

Furthermore, the model has to be modified to give a better description of the PCB temperature. By including the heating of the PCB by other components, the temperatures will get values closer to reality and the heat flow in the bond wires will be reduced. In order to do this, a better knowledge of the heating by other components is needed. Alternatively, a study of how the temperature of the PCB varies with the change in temperature of the surrounding gas could be performed. The boundary conditions of the envelope surface of the PCB can then be changed from insulation to specified temperature, which would give a more reliable model.

When this knowledge is obtained, it is possible to simulate how different changes affect the thermal properties. Simulations can be made in order to investigate how the power consumption of the heaters can be minimized. The geometry can be studied, and relevant questions to ask are how the size of the chip, the radius of the bond wires and the geometry of the glass carrier influence the system. The glass carrier is an important insulator, but can it be made more efficient by changing the geometry? Furthermore, a closer investigation of how the orientation of the module affects the system can be made. No change in the power consumption is observed experimentally, but theoretically the orientation is of importance. Simulations of other material properties, in order to find out how the system is altered, are interesting. How the gas composition and presence of water vapor influence the module can also be studied.

It would be valuable to do a time-dependent study of the sensor system. Assuming that a model for the convection has been developed, an extension of the

existing FEMLAB model can be made. Initial conditions have to be defined and the general heat equation can be solved. It is possible however, to start out from the empirical model developed in this diploma work and do a time-dependent simulation of the system.

Bibliography

[1] AirBorn Electronics. *http://www.airborn.com.au/method/fr4pcb.html*, May 2005.

[2] AppliedSensor. *http://www.appliedsensor.com*, April 2005.

[3] Peter Atkins and Loretta Jones. *Chemical Principles - The Quest for Insight*. Freeman, 1999.

[4] Gary L. Borman and Kenneth W. Ragland. *Combustion Engineering*. McGraw-Hill, 1998.

[5] Yunus A. Cengel. *Heat Transfer: A Practical Approach*. McGraw-Hill, 1998.

[6] Yunus A. Cengel and Robert H. Turner. *Fundamentals of Thermal-Fluid Sciences*. McGraw-Hill, international edition, 2001.

[7] COMSOL. *FEMLAB 3.1 Documentation*, 2004.

[8] Figus Primore. *http://www.frigprim.com/online/cond_pcb.html*, January 2005.

[9] Igor S. Grigoriev and Evgenii Z. Meilikhov, editors. *Handbook of Physical Quantities*. CRC Press, 1997.

[10] Kirk D. Hagen. *Heat Transfer with Applications*. Prentice Hall, 1999.

[11] J.P. Holman. *Heat Transfer*. McGraw-Hill, 9th edition, 2002.

[12] Frank P. Incropera and David P. DeWitt. *Fundamentals of Heat and Mass Transfer*. Wiley, 5th edition, 2002.

[13] Carl Nordling and Jonny Österman. *Physics Handbook for Science and Engineering*. Studentlitteratur, 6th edition, 1999.

[14] Niels Ottosen and Hans Petersson. *Introduction to the Finite Element Method*. Prentice Hall, 1992.

[15] Bruce E. Poling, John M. Prausnitz, and John P. O'Connell. *The Properties of Gases and Liquids*. McGraw-Hill, 5th edition, 2001.

[16] Alf Samuelsson and Nils-Erik Wiberg. *Finite Element Method - Basics*. Studentlitteratur, 1998.

[17] Gilbert Strang and George J. Fix. *An Analysis of the Finite Element Method*. Prentice Hall, 1973.

[18] H. Y. Wong. *Handbook of Essential Formulae and Data on Heat Transfer for Engineers*. Longman, 1977.

Appendix A

Gas Properties

A.1 Volume, Mole and Mass Fraction

The gas sensor measures the concentration of hydrogen in volume fraction. The relations between volume, mole and mass fractions will be described in this section.

The ideal gas law states [13]:

$$pV = nRT \ , \tag{A.1}$$

where p is the pressure, V is the volume, n is the number of moles, R is the molar gas constant and T is the temperature. The volume and mole fractions for an ideal gas will therefore be identical. It is assumed that the volume and mole fractions are the same in the sensor model.

The relation between mole and mass fractions are to be considered next. First, consider 1 mole gas. Each component has a mass equal to the mole fraction times the molar mass, and therefore the mass fraction for component i becomes:

$$\text{mass fraction}(i) = \frac{\text{mole fraction}(i)M(i)}{\sum_j \text{mole fraction}(j)M(j)} \ . \tag{A.2}$$

Next, consider 1 kg gas. Each component consists of the mass fraction divided by the molar mass moles. The mole fraction for component i is then:

$$\text{mole fraction}(i) = \frac{\text{mass fraction}(i)/M(i)}{\sum_j \text{mass fraction}(j)/M(j)} \ . \tag{A.3}$$

A.2 Numerical Values of Gas Properties for Different Temperatures

The density, the specific heat capacity, the thermal conductivity and the viscosity of nitrogen, oxygen and hydrogen for different temperatures can be found in [11]. In tables A.1 - A.3 the gas properties for the temperature range $200 - 500$ K is accounted for. The temperature range is chosen to include all possible values of the temperature of the gas, defined in section 2.4.

Temperature $[K]$	ρ $[\frac{\text{kg}}{\text{m}^3}]$	c_p $[\frac{\text{kJ}}{\text{kgK}}]$	k $[\frac{\text{W}}{\text{mK}}]$	μ $[\frac{\text{kg}}{\text{ms}}]$
200	1.7108	1.0429	0.01824	$12.947 \cdot 10^{-6}$
300	1.1421	1.0408	0.02620	$17.84 \cdot 10^{-6}$
400	0.8538	1.0459	0.03335	$21.98 \cdot 10^{-6}$
500	0.6824	1.0555	0.03984	$25.70 \cdot 10^{-6}$

Table A.1: Properties of nitrogen.

Temperature $[K]$	ρ $[\frac{\text{kg}}{\text{m}^3}]$	c_p $[\frac{\text{kJ}}{\text{kgK}}]$	k $[\frac{\text{W}}{\text{mK}}]$	μ $[\frac{\text{kg}}{\text{ms}}]$
200	1.9559	0.9131	0.01824	$14.85 \cdot 10^{-6}$
250	1.5618	0.9157	0.02259	$17.87 \cdot 10^{-6}$
300	1.3007	0.9203	0.02676	$20.63 \cdot 10^{-6}$
350	1.1133	0.9291	0.03070	$23.16 \cdot 10^{-6}$
400	0.9755	0.9420	0.03461	$25.54 \cdot 10^{-6}$
450	0.8682	0.9567	0.03828	$27.77 \cdot 10^{-6}$
500	0.7801	0.9722	0.04173	$29.91 \cdot 10^{-6}$

Table A.2: Properties of oxygen.

Temperature $[K]$	ρ $[\frac{\text{kg}}{\text{m}^3}]$	c_p $[\frac{\text{kJ}}{\text{kgK}}]$	k $[\frac{\text{W}}{\text{mK}}]$	μ $[\frac{\text{kg}}{\text{ms}}]$
200	0.12270	13.540	0.1282	$6.813 \cdot 10^{-6}$
250	0.09819	14.059	0.1561	$7.919 \cdot 10^{-6}$
300	0.08185	14.314	0.182	$8.963 \cdot 10^{-6}$
350	0.07016	14.436	0.206	$9.954 \cdot 10^{-6}$
400	0.06135	14.491	0.228	$10.864 \cdot 10^{-6}$
450	0.05462	14.499	0.251	$11.779 \cdot 10^{-6}$
500	0.04918	14.507	0.272	$12.636 \cdot 10^{-6}$

Table A.3: Properties of hydrogen.

Appendix B

Convection Coefficient of Bond Wires

In section 3.4.1, the negligence of the convection in the bond wires is justified. Numerical values of the convection coefficient for the bond wires are used, and the computation is presented here.

The bond wires are considered as vertical cylinders with small diameter. The Nusselt number can then be expressed by [18]:

$$\mathrm{Nu} = 0.686(\mathrm{GrPr})^{\frac{1}{4}}[\frac{\mathrm{Pr}}{1+1.05\mathrm{Pr}}]^{\frac{1}{4}} \ . \tag{B.1}$$

The only thing specific for the bond wires is the Nusselt number. The rest of the computation is based on the formulas presented in section 6.1.